Origin of negative Cerium anomalies in subduction-related volcanic samples: constraints from Ce and Nd isotopes

Nina Bellot, Maud Boyet, Régis Doucelance, Pierre Bonnand, Ivan Savov, Terry Plank, Tim Elliott

Origin of negative Cerium anomalies in subduction-related volcanic samples: constraints from Ce and Nd isotopes

Nina Bellot [a], Maud Boyet [a], Régis Doucelance [a], Pierre Bonnand [a], Ivan P. Savov [b], Terry Plank [c], Tim Elliott [d]

[a] Université Clermont Auvergne, CNRS, IRD, OPGC, Laboratoire Magmas et Volcans, F-63000 Clermont-Ferrand, France.

[b] *School of Earth and Environment, Institute of Geophysics and Tectonics, University of Leeds, Leeds LS2 9JT, UK.*

[c] *Lamont-Doherty Earth Observatory of Columbia University, 61 Route 9W, Palisades, New York 10964, USA.*

[d] *Bristol Isotope Group, School of Earth Sciences, University of Bristol, Wills Memorial Building, Queen's Road, Bristol BS8 1RJ, UK.*

Corresponding author: maud.boyet@uca.fr

nina.bellot.gmail.com / r.doucelance@opgc.fr / pierre.bonnand@uca.fr/

i.savov@see.leeds.ac.uk / tplank@ldeo.columbia.edu / tim.elliott@bristol.ac.uk

Main text: 8952 words (without abstract, references, table and figure captions)

Figures: 11

Tables: 3

Supplementary files: 7

ABSTRACT

Negative Cerium (Ce) anomalies are observed in chondrite-normalized rare earth element patterns from various volcanic arc suites. These anomalies are well defined in volcanic rocks

from the Mariana arc and have been interpreted as the result of addition of subducted sediments to the arc magma sources. This study combines $^{143}Nd/^{144}Nd$ and $^{138}Ce/^{142}Ce$ isotope measurements in Mariana volcanic rocks that have Ce anomalies ranging from 0.97 to 0.90. The dataset includes sediments sampled immediately before subduction at the Mariana Trench (Sites 801 and 802 of ODP Leg 129) and primitive basalts from the Southern Mariana Trough (back-arc basin). Binary mixing models between the local depleted mantle and an enriched end-member using both types of sediment (biosiliceous and volcaniclastic) found in the sedimentary column in front of the arc are calculated. Marianas arc lavas have Ce and Nd isotopic compositions that require less than 2.5% of a sediment component derived from the volcaniclastics. With this proportion of sediment, most of the Ce/Ce* range measured in lavas is reproduced. Thus, this study confirms that the origin of the Ce anomalies in the Mariana arc magmas can be principally attributed to recycling of trench sediments through active subduction. The participation of a component derived from biosiliceous sediments does not explain the Ce-Nd isotope composition of the lavas because the involved proportion is too high (up to 8%) in comparison to results obtained from other geochemical proxys. Using this end-member, the modeled Ce anomalies are also too high (0.91-0.84) in comparison to those measured in lavas. Various processes and conditions are able to generate Ce anomalies: oxygen fugacity, residual mineral phases, partial melting, fractional crystallization and tropical weathering. Their influence in the case of Mariana volcanic arc magmas seems to be very limited but partial melting effect may explain the lowest measured Ce/Ce* values. Magmatic processes cannot be definitely ruled out in producing Ce anomalies in other arc system environments. Additional experimental data, however, are needed for a better understanding of the behavior of cerium relative to its neighboring elements. Also, this study highlights the importance of using local depleted mantle and sediments to model the isotopic compositions of arc lavas.

Highlights:

- Origin of negative Ce anomalies in Mariana arc magmas.

- Coupled $^{138}Ce/^{142}Ce$ and $^{143}Nd/^{144}Nd$ isotope measurements in Mariana arc magmas, sediments and back-arc basalts.
- Ce-Nd isotopic binary mixing models coupled with Ce/Ce* prove that volcaniclastic sediments control the Ce/Ce* in Mariana lavas.

Keyword: Ce anomalies, $^{138}Ce/^{142}Ce$, sediment recycling, Mariana volcanic arc, Rare Earth Elements.

1. Introduction

Arc magmas record chemical signatures associated with subduction processes. The subducted slab inventory is made up of variously altered and different in age subducted oceanic crust and its sedimentary cover. The sediments are diverse in type and origin depending on the age of the subducting plate, proximity to a continent, and the presence or absence of an accretionary prism (Plank and Langmuir, 1998a; von Huene and Scholl, 1991). Cerium anomalies have been measured in arc rocks from different localities, particularly the New Britain, Mariana, Tonga, Central America and the Lesser Antilles (Carr et al., 1990; Dixon and Batiza, 1979; Ewart et al., 1973; Jakes and Gill, 1970; White and Patchett, 1984). A negative Ce anomaly means that the Ce concentration normalized to the chondritic value is lower than the value interpolated from the two neighboring Rare Earth Elements (REE) Lanthanum (La) and Praseodymium (Pr). The origin of negative Ce anomalies in arc settings has been attributed to the addition of sedimentary component to the arc magma source (Dixon and Batiza, 1979; Elliott et al., 1997; Hole et al., 1984; Woodhead, 1989). Cerium is the only REE that exists in either 3^+ or 4^+ oxidation states and in nature Ce fractionations are related to the changes of the redox conditions. The short residence time of Ce^{4+} in seawater relative to the trivalent Ce^{3+} ions explains the large negative Ce anomaly in the seawater REE pattern (Elderfield and Greaves, 1982). Fe-Mn crusts and MnO clays preferentially scavenge Ce^{4+} relative to other REE^{3+} and thus have positive Ce anomalies (Amakawa, 1991; Bau et al., 2014). Conversely, negative Ce anomalies are generally identified in authigenic clays,

hydrothermal sediments, nannofossil ooze, or fish debris (Moiroud et al., 2015; Picard et al., 2002; Plank and Langmuir, 1998). The geochemical composition of subducting sediments is now fairly well known globally (Plank, 2013). However, the average "global subducting sediment" reservoir (GLOSS, see Plank and Langmuir (1998) and Plank (2013)) does not show significant Ce anomaly with Ce/Ce* values of 0.97 and 1.02 for GLOSS I and GLOSS II, respectively. The majority of the mean trench sedimentary piles in individual subduction zones used for the GLOSS reservoir calculation have negative Ce/Ce* values (57% of them based on the weighted mean composition of each pile). The lack of anomaly in GLOSS reflects the dominance of volcanic ashes and turbidites in some trench sediments that represent large masses in the total budget, which are deposited too quickly to fractionate Ce from other REE.

The ^{138}La-^{138}Ce isotope systematics ($T_{1/2}$ = 292.5 Ga; Tanimizu, 2000) is an interesting tool to trace the recycling of sediments in subduction zones since material characterized by Ce anomalies have fractionated La/Ce ratios and then will develop by radiogenic ingrowth different ^{138}Ce/^{142}Ce ratios. Calculations show that significant deviations of the ^{138}Ce/^{142}Ce ratio from the chondritic reference can be generated in less than 100 Ma in sediments characterized by highly fractionated La/Ce ratios (3-8) as those measured in seawater (see Figure 1 in Bellot et al., 2015). Thus, combining the ^{138}La-^{138}Ce and ^{147}Sm-^{143}Nd systematics in magmatic arc samples may offer a unique opportunity to better characterize the nature of the sediments involved in the magma genesis because these sediments are characterized by different REE patterns and evolve to distinct ^{138}Ce/^{142}Ce and ^{143}Nd/^{144}Nd isotopic signatures. The Mariana arc is an ideal test site because this arc-basin subduction system is of intra-oceanic type (located >2000 km away from continents) experiencing no terrigeneous (crustal) inputs to its trench sediments. Moreover, the plate entering into subduction is one of the oldest at the Earth's surface (~ 170 Ma old; Bartolini and Larson, 2001; Koppers et al., 2003). On average the sedimentary material at the Mariana Trench is characterized by a large negative Ce/Ce* values of 0.73 (Plank, 2013) and sediments drilled on the fore-arc area show ages up to 170 Ma (Karpoff, 1992). During this period the subducted material will develop a radiogenic ^{138}Ce/^{142}Ce signature. The increase is +0.7 epsilon unit considering the average

La/Ce ratio estimated for the bulk sedimentary column whereas the excess is +1.5 ε-unit for sediments characterized by the strongest La/Ce ratios (>0.85). Finally the Mariana Islands have been extensively studied with the aim of characterizing the nature of outfluxes originating from the subducting slab (e.g. Chauvel et al., 2009; Elliott et al., 1997; Freymuth et al., 2015; Gribble et al., 1998; Hole et al., 1984; Ishikawa and Nakamura, 1994; Martindale et al., 2013; Meijer, 1976; Meijer and Reagan, 1981; Moriguti and Nakamura, 1998; Ribeiro et al., 2015; Savov et al., 2005, 2007; Snyder et al., 2004; Stolper and Newman, 1994; Straub, 2003; Tollstrup and Gill, 2005; Wade et al., 2005; Woodhead et al., 2012; Woodhead, 1989, 1988; Woodhead and Fraser, 1985). The correlation observed between Ce/Ce* and several other proxys (i.e. Ba/La, $^{143}Nd/^{144}Nd$) confirms that the negative cerium anomalies measured in Marianna lavas are likely to be inherited from the sedimentary component rather than reflecting the process by which it was transferred (Elliott et al., 1997). Here we present La-Ce and new Sm-Nd isotope measurements in arc lavas coming from the Mariana Islands (Central Island province), in sediments sampled in front of the subduction trench, and in basalts from the back-arc area. We discuss the origin of negative cerium anomalies with respect to $^{138}Ce/^{142}Ce$ and $^{143}Nd/^{144}Nd$ isotope ratios and then extend our conclusions to the whole database of samples collected in the context of subduction zone for which combined Ce and Nd isotope measurements are available.

2. Geological settings and sample selection

The Mariana volcanic arc represents the southern segment of the Izu-Bonin-Mariana (IBM) arc-basin system, which results from the > 50 Ma of subduction of the Pacific plate under the Philippine Sea plate. The subducting Pacific plate is Jurassic (~ 170 Ma old; Bartolini and Larson, 2001; Koppers et al., 2003), making it the oldest subducted oceanic slab. Its subduction rate is relatively slow (~4 cm/yr) (Seno, 1977; Stern et al., 2003). The IBM volcanic arc is 2800 km long and extends from Mt. Fuji volcano on the Japanese peninsula to the island of Guam in the south. The Mariana arc can be divided into three well-defined zones: the fore-arc, the magmatic front and the back-arc basin or the Mariana Trough (Figure

1). The Mariana fore-arc corresponds to the area between the trench and the magmatic arc front and is characterized by lack of accretionary sedimentary prism i.e. all sediments and underlying Pacific oceanic crust are effectively subducted. The magmatic front of the Mariana arc includes around 40 active volcanoes (Pearce et al., 2005), many of which are currently submerged. The volcanic activity over the last two centuries has been sub-aerial in the central part and underwater in the northern and southern arc segments. The western segment of the arc forms the actively spreading back-arc: the Mariana Trough. The opening of this back-arc basin is related to intra-arc rifting due to tectonic forces associated with the NW subduction of the Pacific plate and the rotation and spreading within the Philippine Sea plate (Stern et al., 2003). The back-arc converges in the south and north with the magmatic arc front (see Figure 1). The maximum back-arc basin width is 100 km in the center (Pearce et al., 2005). The magmatic activity in the back-arc results from adiabatic decompression melting due to seafloor extension combined with fluid mediated melting (Kelley et al., 2010). The back-arc basalt compositions are either MORB-type or arc-type basalts, depending on the proportion of fluids coming from the subducted slab that have been introduced into the otherwise highly depleted sub-arc mantle underneath (Gribble et al., 1996; Pearce et al., 2005; Savov et al., 2005, 2007; Stolper and Newman, 1994; Taylor and Martinez, 2003; Volpe et al., 1987; Woodhead et al., 1993).

Twelve fresh basaltic to basaltic-andesite samples from the Mariana central island arc volcanic province have been selected for this study (Figure 1). A more detailed description of these samples is found in Elliott et al. (1997), who report the major-, trace-element concentrations and Th, Sr, Pb and Nd isotopic compositions of the same samples. In addition, several studies regarding the stable isotope ratios of those same samples are available in the literature (Bouman et al., 2004; Eiler et al., 1997; Freymuth et al., 2015; Prytulak et al., 2013a, 2013b; Savage et al., 2010; Williams et al., 2018).

Ocean drilling program (ODP) sites 800, 801 and 802 were drilled during Leg 129 seaward of the Mariana arc. The drilling aim was to sample the altered Pacific crust and its Jurassic-to-present sedimentary cover (Larson and Lancelot, 1992). The samples recovered

from Site 801 currently represent the primary reference site for subducted inputs to the Mariana arc (Pigafetta basin and East Mariana basin located in Figure 1; see Plank (2013) and references therein for details). The sedimentary column at Site 801 documents the plate's voyage northwestward across the Pacific (Karpof, 1992), initially accumulating red clays (Unit V) in the Jurassic, followed by radiolarites (Unit IV) when passing beneath the high productivity belt at low latitudes. The biosiliceous accumulations of Units IV and II are interrupted by intervals of volcaniclastic turbidite deposition (Unit III), due to underwater lava flow outpourings and flank collapses of nearby seamounts in the mid-Cretaceous (Salimullah, 1992). The last 50-60 Ma of sediment deposition are condensed within the upper 50 meters of the site 801 in Unit I, which is composed of pelagic red clay, recording periods when the site entered the barren central gyre of the Pacific, far from terrigeneous inputs and low in biologic productivity. Thus, most of the sedimentary section is composed of biosiliceous cherts and radiolarites and Cretaceous volcaniclastics, all selected to be studied here (8 samples from Site 801 and 2 additional volcaniclastics from Site 802 to the south). A detailed description and the stratigraphic section at Site 801 are given in Figure 2 and Table 1, together with the location of our samples. The samples analyzed here are representative of the entire range in Ce anomaly (Figure 2).

Basalts from the Mariana Trough (MTB) sometimes have trace elements and water contents similar to those of Mid-Ocean Ridge Basalts (MORB). The majority of them however is likely to be contaminated by fluids from the subducted Pacific slab. In this case samples are enriched in fluid mobile elements (Rb, Ba, K and Pb), and therefore have intermediate compositions between MORBs and arc lavas (Pearce et al., 2005). Our southern MTB samples were recovered during the Cook 7 expedition (R/V Melville-2001) from an area along the back-arc spreading axis that is ~4 km under sea level and where the distance between the spreading center ridge and the magmatic arc front decreases from 106 to 33 km (Figure 1), providing the means to probe the relation between back-arc magmatism and the adjacent volcanic arc front. Three southern MTB samples have been analyzed for both REE contents and Ce-Nd isotopes.

Finally, three Pacific MORB samples (unaltered glasses) have been analyzed as proxy for the background upper mantle isotopic composition. The Searise-1 DR05 sample was dredged during the Searise-1 cruise in 1980 (2.28°N-102.78°W), the Cyana CY82 sample is a submersible-collected sample from the Cyana expedition in 1982 (12.72°N-103.91°W) and the Clipperton DR01 sample (dredge) is from the Clipperton cruise in 1981 (12.75°N-103.93°W). Two additional Pacific MORB samples were previously analysed at the Laboratoire Magmas et Volcans (LMV) and published in Bellot et al. (2015). All these samples do not show any anomalous characteristics in terms of mantle heterogeneity (they all have similar REE patterns and they do not show any DUPAL signature) nor do they indicate a deep mantle signature based on their Hf and Nd isotope ratios (Chauvel and Blichert-Toft, 2001).

3. Analytical procedures

REE concentrations of all Mariana samples (arc basalts and Mariana Trough basalts), of MORB sample Searise-1 DR05 and of 3 of the sediments (801B-12R, 802B-19 and 802B-43R) were measured at LMV Clermont-Ferrand. All other REE data are from the literature (see Table 1). In order to determine the REE concentrations, 100 mg of each sample were digested in Savillex© beakers in a 3:1 mixture of 48% HF and 65% HNO_3 for 48 hours at 75°C. Before evaporation, 200 µl of $HClO_4$ acid were added to expel the fluorides. For sedimentary samples, a preliminary degassing procedure using a 7M-HNO_3:2M-HCl mixture was carried out in order to destroy the potentially carbonated and calcic components (Carpentier, 2007). After the dissolution, samples were dissolved in 6M HCl and a 5% aliquot was uptaken for the measurement of REE concentrations whereas the remaining 95% of the sample was used for Ce and Nd isotope measurements. For REE measurements samples were firstly dissolved in 7M HNO_3 to obtain a dilution factor of ~250, and measurements on the Inductively Coupled Plasma Mass Spectrometer (ICP-MS) were performed with a final dilution factor of 3500 in 0.45M HNO_3 – 0.05M HF. Two rock standards (Icelandic basalt BIR-1 and Hawaii basalt BHVO-2) and one blank were dissolved using the same procedure. Measurements were performed using the LMV Agilent 7500 quadrupole mass-spectrometer.

All calculations to transform peak signals into concentrations were performed offline. A blank, bulk rock standards and a synthetic solution (CMS) containing ~ 60 trace elements at 1 ppb were run every 4 Mariana samples throughout the entire sequence.

The Ce chemical separation protocol, described in detail in Bellot et al. (2015), requires three steps: 1) isolation of the REE from the major elements which is carried out on AGW50-X8 resin using 2.5M and 4M HCl acids; 2) the Ce and the Nd are separated on an AGW50-X8 resin using 0.27M 2MLA (α-hydroxyisobutyric) acid; and finally 3) the Ce fraction is purified from residual Nd on Ln-Spec resin using 0.2 M HCl acid. The Nd fraction collected on the second column is purified from Sm using a Ln-Spec resin and 0.25 M HCl (Pin and Santos Zaldueguilt, 1997). Cerium and Nd blanks were regularly measured by ICP-MS. The Nd blanks were in the range of 22-39 pg whereas Ce blanks were between 44 and 339 pg. Those values are negligible relative to the large quantity of Nd and Ce (> 1μg) processed for each sample.

Cerium and Nd isotopes were measured using a Thermo Scientific Triton Thermal-Ionization Mass Spectrometer (TIMS) at the LMV in Clermont-Ferrand. Instrumental mass bias effects on Nd were corrected using an exponential law and $^{146}Nd/^{144}Nd=0.7219$ (Hamilton et al., 1983). Repeated measurements of the JNdi-1 Nd standard during the course of this study gave an average $^{143}Nd/^{144}Nd$ ratio of 0.512107±4 (2 standard deviation (2SD); n = 14) in agreement, within error, with the value published in Tanaka et al. (2000). The Ce isotope compositions were analyzed as oxide species using double Re filaments (Bellot et al., 2015; Doucelance et al., 2014). The potential interferences of Ba, La, Pr and Nd were monitored during the TIMS measurements. In oxide forms they are always negligible. The purity of the Ce fraction after the chemistry was always checked by ICP-MS before isotope analysis. The signal measured by ICPMS in our samples for La, Pr and Nd was similar to the blank level showing that the Ce purification is faultless. Cerium isotope ratios were corrected for the mass bias using an exponential law and $^{136}Ce/^{142}Ce = 0.01688$ (Makishima et al., 1987). The $^{138}Ce/^{142}Ce$ analyses were carried out during 4 analytical sessions. The ^{140}Ce tailing effect was quantified in each session because of its variability through time (Bellot et

al., 2015). Here we note a tailing correction on the $^{138}Ce/^{142}Ce$ ratio that varies from 0.5 to 1.2 ε-unit after mass bias correction. The Ce reference material solution AMES was measured at least once a day for Ce isotopes (between 5 and 19 times for each session; Supplementary file A). The drift of 49 ppm for the mean AMES $^{138}Ce/^{142}Ce$ ratio between the 4 sessions is attributed to ageing of the Faraday cup. The AMES mean $^{138}Ce/^{142}Ce$ ratios have been normalized to 0.0225746±9, a value obtained with the LMV TIMS for this standard during a previous analytical session in which chondrites were measured to define the Chondritic Uniform Reservoir (CHUR) reference value (Bellot et al., 2015). The epsilon value for this standard solution is 4.13. The same AMES reference material analyzed by Willbold (2007) and Willig and Stracke (2017) gave $^{138}Ce/^{142}Ce$ ratios of 0.0225749±5 and 0.0225747±5 respectively, in good agreement with our measurements. The external reproducibility (2SD) calculated from the repeated AMES measurements within one session is in the range of 0.39 to 0.57 ε-unit (n=19 to 5; Supplementary file A). The Ce reference material solution JMC-304 measured during session 1 gave a $^{138}Ce/^{142}Ce$ ratio of 0.0225704±11 (εCe= 2.22±0.51 (2SD); n=3, Supplementary file A). The Hawaii basalt standard BHVO-2 was measured during session 2 and its $^{138}Ce/^{142}Ce$ is 0.0225643±3 (εCe= -0.49±0.13).

4. Results

4.1. Cerium anomalies in Mariana arc

REE concentrations measured in Mariana lavas, as well as in Mariana Trough Basalts, sediments and Pacific MORBs are presented in Table 1. REE concentrations in sediments are from literature (Vervoort et al., 2011) except three sedimentary samples (801B-12R, 802A-19R and 802A-43R) that have been analyzed here (Table 1). USGS BHVO-2 (Hawaii basalt) reference material was used to calibrate the signal considering the compilation given in the GeoReM online database of Chauvel et al. (2011). Results obtained for the USGS BIR-1 (Icelandic basalt) standard are in agreement with certified values, with a difference of less than 5% in REE, and the external reproducibility (2SD) estimated from 4 measurements is between 1% for Nd and 4% for Eu. In order to calculate the Ce anomaly, two methods of

calculation have been compared (Supplementary file B): 1) using the concentrations calculated with the BHVO-2 standard as calibrator; 2) by calibrating the signal relative to the CMS solution. They give consistent results with differences always smaller than 0.02 on the cerium anomaly. Results obtained with the first calculation method are used in the discussion. The Ce/Ce* (Ce_N / ($La_N^{0.5}$ x $Pr_N^{0.5}$)) values calculated for the two USGS rock standards BIR-1 and BHVO-2 using the second method of calibration are equal to 0.961±0.006 (2SD, n=4) and 1.005±0.006 (2SD, n=4), respectively, which corresponds to a reproducibility better than 1%. Moreover, our BIR-1 results are in excellent agreement with the values of 0.957±0.027 (2SD, n=6) published by Chauvel et al. (2011). A compilation of BIR-1 measurements is reported in Pourmand et al. (2012) and the Ce anomaly in this rock standard is comprised between 0.93 and 0.99 (average value of 0.96±0.04, 2SD, n=11). BIR-1 and BHVO-2 Ce anomalies are also consistent with the Ce/Ce* values calculated from certified concentrations: 0.97 and 1.01 for BIR-1 and BHVO-2, respectively. Our trace element data for Mariana arc samples are in excellent agreement within 2% with values published by Elliott et al. (1997) (Supplement file C). The Ce anomalies in Mariana arc lavas are all negative, ranging from 0.90 to 0.97. There is a 1% offset to higher Ce/Ce* in the values determined here in comparison to previous published values, perhaps due to Ca perchlorate interference on the light REE (Longerich, 1993) or slight differences in the calibration values for BHVO-2. Sediments show a larger range in Ce/Ce* than lavas. They vary from 0.59 in sample 801A-8R to 1.06 in sample 802A-19R.

4.2. Ce and Nd isotopes

The measured $^{138}Ce/^{142}Ce$ and $^{143}Nd/^{144}Nd$ ratios for Mariana arc samples, Mariana Trough Basalts, Mariana trench sediments and the selected Pacific MORBs are presented in Table 2. They are currently expressed in the epsilon notation (see Table 2 for values and calculations). The Mariana arc samples have negative ε_{Ce} ranging from -0.84 (GUG-6) to -0.45 (URA-7). The ε_{Nd} values of the same samples range from 6.01 (GUG-3) to 8.07 (GUG-

9). The MORB samples have ε_{Ce} from -1.65 to -0.77 and ε_{Nd} between 9.69 and 10.56, with mean values of -1.08 and 9.99 for ε_{Ce} and ε_{Nd}, respectively. The isotope data we report here is in good agreement with previous measurements of Ce isotopes in MORBs, whose mean ε_{Ce} is -0.90 and mean ε_{Nd} is 9.73 (Bellot et al., 2015; Doucelance et al., 2014; Makishima and Masuda, 1994). The three MTB samples yield heterogeneous Ce and Nd isotopic compositions. Sample D68-2-1 has Ce and Nd isotopic compositions similar to that of MORB end-member (ε_{Ce}= -1.13; ε_{Nd}= 9.79). The two other back-arc basalts have compositions similar to those of the basaltic Mariana arc lavas. Isotope results are consistent with the conclusions of Pearce (2005) based on trace-element measurements since D68-2-1 was the only analysed sample collected in a segment of the south Mariana Trough that was identified as a MORB-like domain, *i.e.* without contamination by slab fluids.

For the Mariana trench sediments, the isotopic ratios of volcaniclastic turbidites are quite homogeneous and range from -0.13 to 0.29 and from 0.97 to 5.17 for ε_{Ce} and ε_{Nd}, respectively. The Nd isotope compositions of the same samples were already measured for the 2 volcaniclastic samples 801B-5R and the 801B-8R (Vervoort et al., 2011). Our results are in agreement with these earlier results to within 30 ppm, a difference that can be attributed to powder heterogeneity. In comparison to volcaniclastics, the biosiliceous sediments have more variable Ce and Nd isotope ratios with ε_{Ce} ranging from 0.30 to 1.15 and ε_{Nd} from -8.64 to -0.79. The large isotopic variations in the biosiliceous sediments reflect a broad lithological diversity.

5. Discussion

The lava samples analysed in this study have ε_{Nd} and ε_{Ce} that differ from those of MORB samples. In order to explain such variations, we develop mixing models between the local, depleted mantle and two distinct components derived from recycled sediments. In a second

step, we detail other potential factors that could influence the rare earth element contents of the lavas and potentially generate Ce anomalies..

5.1. Ce-Nd isotope constraints on the origin of Ce anomalies in Mariana lavas

Mariana arc samples show a co-variation in ε_{Nd} vs. Ce/Ce* diagram (Figure 3A). The co-variation is less well defined in the ε_{Ce} vs. Ce/Ce* plot (Figure 3B) because the total variation in Ce isotope composition is small. The Sm-Nd systematics confirms that the Ce anomalies are mostly source-related, in agreement with the conclusions of Elliott et al. (1997). Biosiliceous and volcaniclastic trench sediments possess distinct $^{138}Ce/^{142}Ce$ and $^{143}Nd/^{144}Nd$ isotope ratios (Table 2). Thus binary mixing models between the depleted mantle (mantle wedge) and the two types of sedimentary components (biosiliceous *vs* volcaniclastic) may help to better constrain the nature and the proportions of sediments involved in Mariana arc volcanism. Is a specific material responsible for the presence of the Ce anomalies and for the Ce and Nd isotopic compositions in the Mariana arc lavas? For model purpose, no age correction was applied to the sediments. The drilled samples are considered as representative of the subducted sediments involved in the source of the current volcanism at the Mariana arc. The Mariana arc- trench system is of intra-oceanic type and the pelagic background sedimentation is slow. Moreover the fore-arc topography and geophysical imaging reveal that all of the trench sediment is subducted. With these arguments we can assume that the same type of sedimentary material was indeed subducting in the past.

An important input parameter is the light REE (LREE) concentrations of the DMM end-member. Several estimates have been published however we note significant differences in the proposed concentrations. For example the Ce concentration is 1.4 times higher in the DMM composition of Salters and Stracke (2004) when compared with that of Workman and Hart (2005) and these two DMM-models have Ce/Ce* of 1.05 and 0.91, respectively. The Mariana Trough Basalt D68-2-1 collected in a MORB-like domain segment (Pearce et al.,

2005) yields a REE pattern similar to N-MORB (Figure 4) and has no cerium anomaly (Ce/Ce*=1.00). Comparing the different elemental ratios (La/Ce, Ce/Nd, Nd/Pr) in DMM end-members and the sample D68-2-1, we note that the La/Ce ratio shows the greatest difference (9% instead of 2% for Ce/Nd and Nd/Pr). When Ce/Ce* is calculated without considering La (Ce*=(Pr×(Pr/Nd)), Lawrence et al., 2006) the cerium anomaly in Salter and Stracke (2003) DMM disappears (Ce/Ce*=0.99). These observations suggest that the concentration in La in this end-member is too low. The La content in Salters and Stracke (2004) DMM is increased from 0.234 ppm to 0.265 ppm in order to reproduce the La/Ce ratio measured in the basalt D68-2-1 (equal to 0.331). With such a La content the Ce anomaly is removed and the value fits perfectly within the MORB field in the La/Ce *vs.* La plot presented in Salters and Stracke (2004; see their Figure 2). There is no negative Ce anomaly in rocks sampling the depleted mantle in the literature, with rare exceptions that are commonly attributed to seafloor weathering and low temperature processes (e.g. Makishima and Masuda, 1994).

Another important input parameter is the REE content of the sediment-derived component involved in the source of Mariana basalts. We used the estimated P-T conditions of Syracuse et al. (2010) to evaluate the behavior of Ce and Nd under the Mariana volcanic arc. For hydrated metapelites, these conditions correspond to a transition from aqueous fluids to hydrous melts (Hermann and Spandler, 2008). The hydrous melts are the result of partial melting of sediment in the presence of water. The partial melting of sediments leads to more efficient recycling of LREE when compared to the simple sediment dewatering, although experimental data compiled in Plank et al. (2009) show the strong effect of temperature on the solubility of the REE. Most of the experiments reveal that Ce is not fractionated in comparison to its neighboring elements (Martindale et al., 2013; Skora and Blundy, 2012). To our knowledge only the recent study of Tsay et al. (2017), which conducted experiments on the dehydration of an allanite-bearing eclogite at 2.5 GPa and 600-800°C, obtained aqueous fluids characterized by positive Ce anomalies. However the Ce anomalies on the fluid/(bulk) solid partition coefficients are not resolved when the analytical uncertainties are considered. Here results on high-P/high-T experiments on sedimentary materials are used to constrain the behavior of Ce and Nd, and in particular their partition coefficients in each of the two types of

sedimentary materials: biosiliceous sediments from Johnson and Plank (1999) and in volcaniclastics ones from Martindale et al. (2013).

5.1.1. Biosiliceous sediments

The high-P/high-T experiments of Johnson and Plank (1999) used natural pelagic red clay from the eastern Tonga Trench (DSDP site 595). This type of sediment is common amongst the sediments from the Pacific ocean (Plank and Langmuir, 1998). It is also comparable to the red clays of Unit I and to the non-biogenic fraction of Units II, IV and V at Site 801, east of the Mariana arc front (Figure 2). In the calculations, the concentrations measured in the biosiliceous samples (Vervoort et al., 2011; this study) are multiplied by the enrichment factor reported in Table 3. Sediments produced partial melts in these conditions, and not aqueous fluids. They are depleted in REE in comparison to the initial sediment.

Figure 5A shows the binary mixing curves in ε_{Ce}-ε_{Nd} space between D68-2-1 and components derived from the biosiliceous sediments. The two samples 801A-17R and 801B-33R (a porcellanite and a radiolarite, respectively) cover the entire ε_{Ce} biosiliceous sediment range; thus their isotopic compositions are used to constrain those of the two enriched end-members in the calculated mixing curves. Concentrations used in the model correspond to the average concentration of biosiliceous sediments. Both mixing curves pass through the Mariana arc samples within the error bars on the measurements. The incorporation of 2.5% to 8% of melts extracted from biosiliceous sediments reproduces the $^{138}Ce/^{142}Ce$ and $^{143}Nd/^{144}Nd$ ratios of the Mariana arc samples. This model must also explain the Ce/Ce* values measured in the same samples. The calculated Ce/Ce* values are presented in Figure 5B relative to the sedimentary proportions. For the proportion of sedimentary component determined using Ce-Nd isotopes (2.5% to 8%), the calculated Ce/Ce* values in the Mariana arc samples range from 0.91 to 0.84. These values are significantly lower than Ce/Ce* values (up to 0.90) measured in lavas (Figure. 5B). Results are similar when the mean Ce-Nd

isotope composition is considered for the sedimentary end-member (see supplementary material D).

5.1.2. Volcaniclastic sediments

Our calculations are based on the results obtained experimentally by Martindale et al. (2013) on the volcaniclastic sediment 801B-8R3. The Ce, Pr and Nd concentrations of the fluids were calculated considering the partition coefficients in the 850°C-3GPa experiment (see Table 5 of Martindale et al. (2013) and our Table 3) and the concentration in this volcaniclastic sample published in Vervoort et al. (2011). Because enrichment factors are higher than 1, melts are enriched in REE relative to the initial material. The two mixing lines shown in Figure 6A join the local depleted mantle (with an isotopic composition identical to that of D68-2-1) and two distinct enriched end-members which Ce and Nd isotopic ratios correspond to those of the two volcaniclastic sediments with the most extreme Ce isotope compositions (801B-8R3 and 801B-7R, respectively). Concentrations correspond to the mean value of all voclaniclastic samples. Both curves pass through the lava arc samples within the error bars on the Ce isotope measurements. To explain the $^{138}Ce/^{142}Ce$ and $^{143}Nd/^{144}Nd$ ratios of the Mariana arc lavas, 0.75% to 2.75% melt from volcaniclastic sediments is necessary. Such a contribution would produce arc magmas that are characterized by a Ce/Ce* of 0.97 to 0.95 (Figure 6B). These values are in agreement with the majority of cerium anomalies measured in our samples. One of the four studied volcaniclastic samples (802-43R from site 802) has a Ce/Ce* of 0.88, which is significantly lower than those measured in the other three samples (from 0.91 to 1.06). However, this very low Ce/Ce* value is unique among the 13 measured volcaniclastic samples found in the literature, with a range of Ce/Ce* comprised between 0.88 to 1.06 *(N = 13;* Karpof, 1992; Vervoort et al., 2011; this study). The participation in small proportion of the component derived from volcaniclastic sediments satisfies both Ce-Nd isotope compositions and the Ce anomalies of the Mariana arc. Results are similar when the mean Ce-Nd isotope composition of volcanoclastics is considered for the sedimentary end-member (see supplementary material E).

5.1.3. Comparison with previous estimates

Fluids/melts from the most common sediments (biosiliceous and volcaniclastic) drilled off the Mariana Trench at ODP sites 801 and 802 must have directly participated in the arc magma genesis as evidenced by some key trace element abundances characteristic only to sediments (Elliott et al., 1997; Ishikawa and Tera, 1999; Plank and Langmuir, 1998b). Our calculations show that the melting of subducted volcaniclastics contributed smaller Ce anomalies than the biosiliceous ones and the sedimentary proportions calculated from Ce-Nd isotope data are also smaller for voclaniclastics than for biosiliceous sediments (0.75-2.75% against 2.5 to 8%). The participation of sediments in the source of the Mariana arc lavas has been studied using a large range of geochemical tools, including trace elements and isotope systematics and all results converge towards a sedimentary proportion that does not exceed 4% (^{238}U-^{230}Th, ^{147}Sm-^{143}Nd, ^{176}Lu-^{177}Hf, U-Th-Pb) (Avanzinelli et al., 2012; Elliott et al., 1997; Hole et al., 1984; Tollstrup and Gill, 2005; Vroon et al., 1995; White and Dupré, 1986; Woodhead, 1989). Our Ce-Nd results give sedimentary proportions that agree generally well with these previous estimates if the sedimentary component is derived from volcaniclastics whereas the sedimentary proportion can be up to 8% for biosiliceous sediments and then far above the previous estimates. Moreover with biosiliceous sediments we cannot reproduce both the Ce-Nd-isotope compositions and the cerium anomalies of the lavas. It would be interesting to calculate a bulk sediment Ce isotope composition for the ODP site 801 but this is currently impossible because 1) the number of samples analyzed in this study is too small; 2) no samples from unit 1 of this site were analyzed, and 3) published measurements of ^{138}Ce/^{142}Ce ratios in sediments are very scarce and exist only for Lesser Antilles forearc sediments (Bellot et al., 2015). Unfortunately we did not identify any good chemical proxy for the Ce isotope composition of the Mariana Trench sedimentary column.

We also show the importance of considering the compositions of the sediments on the seafloor near to the deep-sea trench. The very low sedimentary melt proportions of 0.4% for

Mariana arc samples calculated in Hole et al. (1984) to explain their Ce anomalies is a direct reflection of the importance of the choice of mixing end-members. They use the PAWMS (Pacific Authigenic Weighted Mean Sediment) representing the mean concentrations for DSDP Leg 34, Hole 314, located on Nazca plate in the east Pacific Ocean. This material has a very large Ce anomaly (Ce/Ce* of 0.2) compared to sediments located seaward of the Mariana arc front. This observation illustrates the caveats of using average global compositions to quantify the sources contributing to subduction zone-related magmas, in agreement with Woodhead et al. (2012).

5.2. Ce anomalies in worldwide magmatic arcs: can other processes generate cerium anomalies?

The compilation of Ce/Ce* measured in arcs from the geochemical database GEOROC reveals that several subduction zones are characterized by volcanic rocks with negative Ce anomalies, i.e. Central America, the Cascades, Izu-Bonin and Mariana arcs (Figure 7). However, sediments drilled within the trench do not have systematically cerium anomalies (e.g. Cascades). Working on databases has the advantage of bringing out trends but here no data filtering has been applied. We are aware that cerium anomalies are small and only rigorous analytical works can reliably quantify these small variations. Also negative Ce anomalies can result from secondary processes when subaerial basalts are exposed to alteration in tropical environments. This has been found for basalts from French Polynesian islands (Cotten et al., 1995). In this case, the negative Ce anomalies in the basalts result from the precipitation of Y-REE rich phosphates concentrating all REE except Ce. Such precipitates remain rare and are not observed in our Mariana samples. The Mariana arc samples have quite similar REE abundances (Table 1) and their chondrite-normalized values fall between 10 and 100 (Log space) in comparison with 1000 as is the case in arc lavas with Y-REE rich phosphate precipitation. Also, the La/Nb, Nd/Zr or Sm/Hf ratios are all similar and not significantly elevated as would be expected with Y-REE rich phosphates (Cotten et al., 1995). Lastly, the Mariana arc samples are all historic or young enough (<350ka) to have

significant U-Th disequilibria, so they should not have experienced such extensive weathering (Elliott et al., 1997).

The formation of cerium anomaly by magmatic processes such as partial melting and/or fractional crystallization has never been thoroughly examined. We test below the potential influence of magmatism on the Ce/Ce* values in the context of the formation of arc lavas. Since coupled Ce/Ce* and εCe data are now available in lavas of two different island arcs (Antilles and Mariana), our calculations have been applied to these particular cases.

5.2.1. Batch melting

The models are based on the proposed slab geometry beneath volcanic arcs by Syracuse and Abers (2006). Beneath the Mariana volcanic arc front the slab depths vary from 172 to 156 km (north-south). The pressure-temperature conditions at these depths are estimated to be 5-5.5 GPa and 780-820°C (model D80 in Syracuse et al., 2010). In the south part of the Lesser Antilles the slab depth is about 140 km corresponding to pressure-temperature conditions of 4-5 GPa and 780°C (model D80 in Syracuse et al., 2010). Under these conditions, melting occurs in the garnet stability field. Thus we have considered a garnet peridotite with the following modal abundance: 55% olivine, 11% clinopyroxene, 25% orthopyroxene and 9% garnet (Rollinson,1993). Because Mariana arc samples and most of those analysed for Lesser Antilles do not have a garnet signature (fractionation between heavy REE), we can also assume that melting continues into the spinel stability field, or that garnet is consumed. A second composition has been then modelled with the reduction of the garnet content from 9% to 6% and by adding 3% spinel. Mantle wedge metasomatism also needs to be integrated into the model. As a first approximation, we consider that the depleted sub-arc mantle was contaminated by 2% of melt extracted from volcaniclastic sediments fluids (case of Mariana) or 5% fluids coming from the partial melting of the GLOSS-II reservoir (case of Martinique Island following the proportion estimated in Bellot et al., 2015). The fluid composition is calculated by applying the bulk solid/fluid partition coefficients measured from the experiments carried out by Martindale et al. (2013) for Mariana and by Johnson and Plank (1999) for Lesser Antilles. We then assume cryptic metasomatism, in which the bulk

chemistry of the mantle wedge is modified by metasomatism but without bulk mineralogical changes. It is likely that the fluid/melt circulation would have resulted in mineralogical reactions and the occurrence of hydrous minerals. These phases would have been consumed immediately by melting and would probably not play any significant role subsequently. In our model the LREE concentrations of the mantle source are those proposed by Salters and Stracke (2004) for the depleted mantle. The bulk partition coefficients (D) of the garnet-spinel peridotite are determined from K_D values proposed by McKenzie and O'Nions (1991) for each basalt/mineral phase proportion. We choose McKenzie and O'Nions K_D values because their study is the only study given all K_D necessary for our model. The change of Ce/Ce*, expressed in ΔCe/Ce* (normalized to the initial composition equal to 100% of partial melt) is plotted against the degree of partial melting (%). Results presented in Figure 8A show that variation is always very small and lower than 0.021. The maximum Ce/Ce* variation is obtained for 2.5% melting. The spinel peridotite composition results in smaller variations than the garnet composition. The change in the sediment proportion (2 to 5%) and its composition (volcaniclastic *vs* GLOSS) does not modify the calculated curves. Partial melting generates small variation of the cerium anomaly and its potential effect has not been considered in the models presented in figures 5B and 6B. The cerium anomaly changes of 0.01 when considering the typical melting degree for arc lavas, i.e. ~10%. Thus the melting process increases the amplitude of the cerium anomaly and can explain the most extreme Ce/Ce* values of (0.90 to 0.92) measured in a few samples.

5.2.2. Fractional crystallization

Results of the fractional crystallization (FC) calculations are presented in figure 8B. The initial magma corresponds to 10% of partial melting of the previously metasomatized depleted mantle (see section 5.2.1 and figure 8A). The crystallizing mineral assemblage used here results from 1) the modelling of Dixon and Batiza (1979) for Mariana (see Table 5 of their paper); and 2) the propositions made in Labanieh et al. (2012) for andesites from Martinique lavas. The bulk LREE solid/melt partition coefficients between the minerals (olivine, cpx, opx,

plagioclase, amphibole, garnet and/or magnetite) and the basaltic melt are calculated from the partition coefficients $D^{basalt/mineral}$ of McKenzie and O'Nions (1991) except $D^{basalt/magnetite}$ for LREE (Luhr and Carmichael, 1980). Because Pr was not measured in this last study, the partition coefficient for this element has been calculated by linear interpolation between La and Nd that are two elements existing only in 3+ valence state using the following equation: $(1/3)*K_DLa+(2/3)*K_DNd$. This calculation shows that FC does not control the cerium anomaly neither for the Mariana arc nor for Martinique samples with variation lower than 0.005 (Figure 8B). The difference in the lava mineralogy for the two arc systems explains the variations observed in the figure 8B.. Several arguments show that FC does not control the trace element composition neither for the Mariana arc nor for Martinique samples. Firstly, most of our rocks plot on a positive straight line on diagrams using the ratios of two incompatible elements such as Th/REE as a function of the concentration of the most incompatible element (Th), suggesting that variations in trace elements are mostly controlled by batch melting rather than FC (Figure 9). In addition, the Ce/Ce* and MgO contents of the arc samples do not co-vary. In these two locations, sample that seem to be more affected by FC do not have the lowest Ce/Ce* value. The influence of FC on the Ce anomalies is thus limited, especially for Mariana lavas. Turning to Martinique lavas, Labanieh et al. (2012) have examined in great detail the effect of the FC process on REE. They showed that amphibole and garnet are able to fractionate REE ratios (e.g. La/Sm) in some particular volcanic complexes of Martinique (Conil, Carbet, Pelée and Gros Ilet). Our calculations, however, show that FC does not significantly fractionate Ce relative to its neighboring elements and does not generate Ce anomaly in the lavas. Indeed these samples do not differ from the others in the figure 9B.

5.2.3. The role of residual accessory mineral phases

The role of residual accessory mineral phases present in subducted sediments has been previously highlighted, in particular to explain the correlation observed between $^{176}Hf/^{177}Hf$ ratios and Hf concentrations in the Izu-Bonin-Mariana arc system (Tollstrup and Gill, 2005). Thus, less than 2% of fluids coming from 25% of partial melting of subducted sediments are

needed, when associated with 0.0025% of residual zircon, to result in the six-fold increase of the Nd/Hf ratio that is expected to explain the Hf anomalies measured in the Mariana arc lavas (Tollstrup and Gill, 2005). Combined ^{238}U–^{230}Th and ^{235}U–^{231}Pa measurements on Mariana lavas show that the main control on U-series in these samples is exerted by accessory phases (allanite, monazite and zircon) present during the recycling of the subducted material (Avanzinelli et al., 2012). Cerium is incompatible with respect to zircon formed in hydrous veins at eclogitic facies conditions (Rubatto and Hermann, 2003). Zircon retains Ce more efficiently than other REE, but its concentrations remain very low in comparison to those observed in magmatic zircons (~2 ppm in zircon veins formed by fluids/melts in subduction zones; Rubatto and Hermann, 2003). If zircon is present during partial melting of the sediments, it might fractionate the HFSE more efficiently when compared to the LREE. The same is true for rutile, whose Ce partition coefficient ($D^{mineral/melt}$) is <0.001 (Klemme et al., 2005). The presence of residual accessory mineral phases in sub-arc conditions can explain the HFSE signatures (Avanzinelli et al., 2012; Martindale et al., 2013), but their influence seems to be limited for the LREE and does not explain any cerium fractionation relative to its neighboring elements. Conversely, the dehydration of an allanite-bearing eclogite seems to produce aqueous fluids characterized by positive cerium anomalies (Tsay et al., 2017), but these anomalies are poorly constrained relative to the analytical precision. Cerium anomaly (Ce/Ce*>1) increases with the temperature of the experiments. This effect cannot be related to a redox effect because experiments made at higher temperature are more reducing, as attested by the amplitude of the Eu anomaly, meaning that the cerium should be present in the valence 3^+ i.e., like the other REE (Tsay et al., 2017). Active serpentinite mud volcanism in the shallow fore-arc region of the Mariana convergent margin presents a unique opportunity to characterize the slab-derived fluids. Here it has been shown that relative to the depleted mantle wedge, the fluid mobile elements which are characteristic of the subducted slabs (B, Cs, I, As, Sb; Snyder et al., 2004; Savov et al., 2005, 2007) are often orders of magnitude more enriched in the serpentinite muds and fluids sampled from carbonate and brucite chimneys at the summits of these mud volcanoes. At the low temperature (<350°C) of the fore-arc regions, the LREE remain immobile as no significant decoupling between Ce, La and Pr has been identified (Savov et al., 2007, 2005).

5.3.1. Effect of mantle redox conditions on Ce valence state

The effect of the oxygen fugacity on the cerium valence state is well known in sub-surface conditions but experiments in mantle conditions are very scarce. The presence of Ce^{4+} in magmatic rocks has been first highlighted with the presence of positive cerium anomaly in zircons. In this mineral the CI-normalized REE pattern is often characterized by the coupled presence of positive cerium and negative europium anomalies. Cerium and Eu, unlike the other REE, do not exclusively form trivalent ions, existing also as Ce^{4+} and Eu^{2+}. The partitioning between zircon and melt for these elements changes with the variations of the oxygen fugacity (Burnham and Berry, 2012). The only other study presenting REE partition coefficients for different reducing conditions is for plagioclase in basaltic melt (Aigner-Torres et al., 2007). The melt in the later study lacks significant cerium anomaly despite the large range of the oxygen fugacity investigated in the experiments (fO_2= IW, QFM, air). However, we note that the plagioclase/melt partition coefficient for cerium does not plot exactly on the 3+ curve in the lattice strain model of Aigner-Torres et al. (2007) but slightly below (see their figure 5). The analytical precision of in-situ REE measurements representing a wide range of relevant experimental conditions does not allow the detection of the Ce anomalies.

The oxidation state of Ce in silicate melt can be quantified using XANES technique (Burnham and Berry, 2014; Smythe and Brenan, 2015). $Ce^{4+}/\Sigma Ce$ in natural melts is exceedingly small and seems to be recorded only in the mineral zircon that has a great potential as an oxy-barometer (Smythe and Brenan, 2016; Trail et al., 2011). Smythe and Brenan (2015) have determined a small fraction of Ce^{4+} under terrestrial magmatic conditions in a large range of fO_2 for rhyolite to basalt compositions (FMQ varying from -4 to +8.4). Using an oxygen fugacity of 2 log units above FMQ as value for magmas in subduction zones (Kelley and Cottrell, 2009; Parkinson and Arculus, 1999), we estimate the Ce^{4+}/Ce^{3+} ratio in a basaltic arc melt of about 0.0012. In addition, in presence of Fe in natural silicate melts, the enthalpy energy of oxidizing Fe ($Fe^{2+} \rightarrow Fe^{3+}$) is lower than the one for Ce (Burnham and Berry, 2014; Schreiber et al., 1980) and the polymerization of the melt increases the redox

state of Ce contrarily to the addition of H_2O (Smythe and Brenan, 2015). In conclusion even if basaltic melts near subduction zones are more oxidized than magmas from divergent plate boundaries (Kelley and Cottrell, 2009), the redox conditions cannot generate Ce anomaly in arc lavas.

The measurement of non-traditional stable isotopes has been developed with the aim of better characterizing the mantle redox conditions. Cations such as Cr, Fe, Ti, and V exhibit a range of valence states that depend on the stability of mineral phases and the partitioning behavior between mineral and melt (Papike et al., 2005). Mariana arc samples have been the subjects of several stable isotope studies, including Tl (Prytulak et al., 2013b), V (Prytulak et al., 2017), Mo (Freymuth et al., 2015) and Fe (Williams et al., 2018). Although some of these analyses were conducted on the Mariana samples studied here, no clear correlation is observed between these isotopes and the Ce isotope ratios. A slight co-variation is observed between Mo and Ce isotopes (n=5). Measured variations in Mo and Ce are too small relative to the analytical errors to be clearly resolved (supplementary file F). Voegelin et al. (2014) showed the absence of fractionation of Mo isotopes ($\delta^{98/95}$Mo) during fractional crystallization in the specific case of Mariana arc magmas since all these samples present a narrow range in MgO concentrations. Molybdenum isotope range in Mariana arc lavas is explained by the participation of fluids from the lower subducted basaltic crust, where Mo isotopes would fractionate during dehydration, and/or by the presence of residual rutile from the sediment melts (Freymuth et al., 2015; Skora et al., 2017). However experimental studies realized so far do not report any Ce fractionation in the presence of residual rutile.

5.3.2 Implications of Ce-Nd isotopes in arc magma environments

The first coupled Ce-Nd isotope measurements on island volcanic rocks were reported for samples characterized by large negative cerium anomalies up to 0.73: 16 samples from two Solomon Islands (Shortland and New Georgia) and 3 samples from Bonin Islands (Shimizu et al., 1992). The compilation of all data available on samples collected in arc settings (lavas,

sediments) and mid-ocean ridge samples is presented in figure 10. We note that lavas from Bonin and Solomon Islands have more radiogenic ε_{Ce} values than those from Mariana and Martinique with comparable ε_{Nd}. Since no sediment collected near Bonin and Solomon Islands has been analyzed, mixing curves cannot be calculated between depleted mantle and enriched source as done for Mariana and Lesser Antilles. Only one enriched end-member composed by sediments having very radiogenic $^{138}Ce/^{142}Ce$ ratios would explain the measured isotope ratios in Bonin and Solomon arc samples. Radiogenic $^{138}Ce/^{142}Ce$ ratios are acquired over time in reservoirs characterized by high La/Ce ratios and then usually having very low Ce contents and much lower Ce/Nd ratios than that of the depleted mantle. With these end-members, mixing calculations produce convex curves in the ε_{Ce} vs. ε_{Nd} diagram that do not pass through the samples located in the upper-right quadrant. Mean sedimentary piles calculated for Izu-Bonin (ODP Leg 185 Site 1149) and Vanuatu (DSDP Leg 30 Site 286) are both characterized by negative cerium anomalies (0.69 and 0.90, respectively) close to that of the sedimentary column sampled at the Mariana trench (0.73). The ε_{Nd} measured in DSDP Leg 30 Site 286 sediments are very high compared to those measured in Mariana (+2 to +9 in Vervoort et al., 2011 and -2 to 10 in Peate et al., 1997). The participation of a large quantity of sediments in the magma source is also excluded from results on Hf, Nd, Sr and Pb isotopes measured in samples from Solomon Islands (Schuth et al., 2009). In conclusion using the geochemical database of oceanic sediments collected in this part of the Pacific Ocean, the cerium isotopic composition of Bonin and Solomon arc samples remains enigmatic. Additionally, we have highlighted the need to use the “local” mantle as depleted end-member in our Ce-Nd isotope mixing models for Mariana samples (Mariana Through basalt instead of the mean MORB). The ε_{Ce} variability in MORB is up to 1.2, which is significant regarding the analytical precision of 0.4. To model Solomon samples, it may be necessary to consider the presence of the Ontong Java plateau and of the Indian mantle wedge trapped under Solomon Islands too. The local tectonic settings result in an anomalously high mantle temperature and probably lead to the production of adakitic melts (Schutl et al., 2009).

Martinique island lavas are of particular interest to understand magma generation in the case of sediment incorporation into the mantle wedge because they all fit on hyperbolas compatible with simple two-component mixtures in isotope variation diagrams (Pb, Sr, Nd and Hf isotope ratios, see Labanieh et al., 2010). However, the cerium anomalies measured in the same samples do not correlate with ε_{Nd} or ε_{Ce} values (Figure 11), even if samples that appear to be significantly affected by fractional crystallization are discarded (see supplementary file G). Samples from Bonin and Solomon Islands studied by Shimizu et al. (1992) show no significant correlation in ε_{Nd}-Ce/Ce* and ε_{Ce}-Ce/Ce* diagrams (Figure 11), and, in a more general way, there is a lack of correlation between ε_{Nd}- and Ce/Ce* in samples from the Izu-Bonin arc (Hochstaedter et al., 2001). This strongly suggests that the cerium anomaly is not always a good proxy of the sediment incorporation in the mantle wedge.

6. Conclusion

The measurement of $^{138}Ce/^{142}Ce$ and $^{143}Nd/^{144}Nd$ on 12 Mariana arc samples, 9 trench sediments from ODP sites 800 and 801, 3 Mariana Trough Basalts and 3 MORB samples provides new information regarding the LREE source of Mariana arc magmas and their negative Ce anomalies. Since the back-arc basalt sample D68-2-1 is representative of the local depleted mantle under the Mariana arc, it is used to model the depleted end-member in the binary mixing calculations. The Ce-Nd binary mixing models were calculated using two different enriched end-members: volcaniclastic sediments and biosiliceous sediments. Our models show that a small proportion of a sedimentary melt derived from volcaniclastic sediments (0.75% to 2.75%) must have been incorporated into the mantle source in order to explain both $^{138}Ce/^{142}Ce$ and $^{143}Nd/^{144}Nd$ ratios of the arc samples and their negative Ce anomalies (0.90 to 0.97). For biosiliceous samples, a too large proportion of a sedimentary melt is required (up to 8%) to explain the Ce-Nd isotope composition of the lavas. Moreover the incorporation of biosiliceous sediments generates too strong Ce anomalies. We highlight

the importance of using local materials, i.e. depleted mantle from the back-arc basin and sediments from ODP sites 801 and 802, in the binary mixing calculations.

Other « magmatic » processes than partial melting and fractional crystallization, that potentially affect Ce anomalies, have been also discussed: these are the influence of oxygen fugacity on the change of valence state of Ce, the presence of residual accessory mineral phases, or the involvement of aqueous fluids resulting from the dehydration of recycled material. The proportion of Ce^{4+} for these redox conditions is extremely low. The precisions on partition coefficient are not sufficient yet to attribute Ce anomaly variations in arc lavas to one of these processes and more experiments are needed at different redox conditions. Their influence on Ce/Ce* are limited in the Mariana arc context, nevertheless they cannot be totally excluded for other arcs.

Comparing the whole database of $^{138}Ce/^{142}Ce$ data available for arc lavas reveals a significant variability between arcs. Bonin and Solomon Island have εCe difficult to explain. A better characterization of the local materials involved in their source together with a better understanding of Ce, and more largely REE, behavior during magmatic processes, may help understanding measured values. Turning to Martinique lavas, their Ce isotope compositions can be explained by a binary mixing between depleted mantle and local sediments, but not their Ce anomalies. So, the link between negative Ce anomalies and sediment additions has to be made carefully and without globalizing the process to all subduction zones.

Acknowledgements

We would like to thank Matthias Willbold and Masaharu Tanimizu for providing us both the Ce-AMES and the JMC-304 reference materials. Thanks to Pierre Schiano for the MORB samples. Help in the chemistry lab provided by Chantal Bosq and with the mass spectrometers by Delphine Auclair and Jean Luc Piro were highly valuable. The paper was also improved by critical comments by W. White and an anonymous reviewer. This research was financed by the French Government Laboratory of Excellence initiative n°ANR-10-LABX-

0006. This project has received funding from the European Union's Horizon 2020 research and innovation programme under Grant Agreement N° 682778. This is Laboratory of Excellence ClerVolc contribution number XXX.

REFERENCES

Aigner-Torres, M., Blundy, J., Ulmer, P., Pettke, T., 2007. Laser Ablation ICPMS study of trace element partitioning between plagioclase and basaltic melts: An experimental approach. Contrib. to Mineral. Petrol. 153, 647–667. doi:10.1007/s00410-006-0168-2

Allegre, C.J., Minster, J.F., 1978. Quantitative Models of Trace-Element Behavior in Magmatic Processes. Earth Planet. Sci. Lett. 38, 1–25.

Amakawa, H., 1991. Isotopic compositions of Ce , Nd and Sr in ferromanganese nodules from the Pacific and Atlantic Oceans , the Baltic and Barents Seas , and the Gulf of Bothnia Earth Planet. Sci. Lett. 105, 554–565.

Avanzinelli, R., Prytulak, J., Skora, S., Heumann, a., Koetsier, G., Elliott, T., 2012. Combined 238U-230Th and 235U- 231Pa constraints on the transport of slab-derived material beneath the Mariana Islands. Geochim. Cosmochim. Acta 92, 308–328. doi:10.1016/j.gca.2012.06.020

Bartolini, A., Larson, R.L., 2001. Pacific microplate and the Pangea supercontinent in the Early to Middle Jurassic. Geology 29, 735–738.

Bau, M., Schmidt, K., Koschinsky, a., Hein, J., Kuhn, T., Usui, a., 2014. Discriminating between different genetic types of marine ferro-manganese crusts and nodules based on rare earth elements and yttrium. Chem. Geol. 381, 1–9. doi:10.1016/j.chemgeo.2014.05.004

Bellot, N., Boyet, M., Doucelance, R., Pin, C., Chauvel, C., Auclair, D., 2015. Ce isotope systematics of island arc lavas from the Lesser Antilles. Geochim. Cosmochim. Acta 168, 261–279. doi:10.1016/j.gca.2015.07.002

Bézos, A., Humler, E., 2005. The Fe3+/ΣFe ratios of MORB glasses and their implications for mantle melting. Geochim. Cosmochim. Acta 69, 711–725. doi:10.1016/j.gca.2004.07.026

Bouman, C., Elliott, T., Vroon, P.Z., 2004. Lithium inputs to subduction zones. Chem. Geol. 212, 59–79. doi:10.1016/j.chemgeo.2004.08.004

Burnham, A.D., Berry, A.J., 2014. The effect of oxygen fugacity, melt composition, temperature and pressure on the oxidation state of cerium in silicate melts. Chem. Geol. 366, 52–60. doi:10.1016/j.chemgeo.2013.12.015

Burnham, A.D., Berry, A.J., 2012. An experimental study of trace element partitioning between zircon and melt as a function of oxygen fugacity. Geochim. Cosmochim. Acta 95, 196–212. doi:10.1016/j.gca.2012.07.034

Carpentier, M., 2007. Composition chimique des sédiments entrant dans la zone de subduction des Petites Antilles. Thèse Université Joseph Fourier.

Carr, M.J., Feigenson, M.D., Bennett, E.A., 1990. Incompatible element and isotopic evidence for tectonic control of source mixing and melt extraction along the Central American arc. Contrib. to Mineral. Petrol. 105, 369–380. doi:10.1007/BF00286825

Chauvel, C., Blichert-Toft, J., 2001. A hafnium isotope and trace element perspective on melting of the depleted mantle. Earth Planet. Sci. Lett. 190, 137–151. doi:10.1016/S0012-821X(01)00379-X

Chauvel, C., Bureau, S., Poggi, C., 2011. Comprehensive Chemical and Isotopic Analyses of Basalt and Sediment Reference Materials. Geostand. Geoanalytical Res. 35, 125–143. doi:10.1111/j.1751-908X.2010.00086.x

Chauvel, C., Marini, J.-C., Plank, T., Ludden, J.N., 2009. Hf-Nd input flux in the Izu-Mariana subduction zone and recycling of subducted material in the mantle. Geochemistry Geophys. Geosystems 10, 1–23. doi:10.1029/2008GC002101

Cotten, J., Dez, A. Le, Bau, M., Caroff, M., Maury, R.C., Dulski, P., Fourcade, S., Bohn, M., Brousse, R., 1995. Origin of anomalous rare-earth element and yttrium enrichments in subaerially exposed basalts: Evidence from French Polynesia. Chem. Geol. 119, 115–138. doi:http://dx.doi.org/10.1016/0009-2541(94)00102-E

Dixon, T.H., Batiza, R., 1979. Petrology and geochemistry of lavas in the northern Mariana: implications for the origin of island arc basalts. Contrib. to Mineral. Petrol. 70, 167–181. doi:10.1007/BF00374446

Doucelance, R., Bellot, N., Boyet, M., Hammouda, T., Bosq, C., 2014. What coupled cerium and neodymium isotopes tell us about the deep source of oceanic carbonatites. Earth Planet. Sci. Lett. 407, 175–186. doi:10.1016/j.epsl.2014.09.042

Eiler, J.M., Crawford, A., Elliott, T., Farley, K.A., Valley, J.W., Stolper, E.M., 2000. Oxygen Isotope Geochemistry of Oceanic-Arc Lavas. J. Petrol. 41, 229–256. doi:10.1093/petrology/41.2.229

Eiler, J.M., Farley, K. a., Valley, J.W., Hauri, E., Craig, H., Hart, S.R., Stolper, E.M., 1997. Oxygen isotope variations in ocean island basalt phenocrysts. Geochim. Cosmochim. Acta 61, 2281–2293. doi:10.1016/S0016-7037(97)00075-6

Elderfield, H., Greaves, M.J., 1982. The rare earth elements in seawater. Nature 296, 214–219.

Elliott, T., Plank, T., Zindler, A., White, W., Bourdon, B., 1997. Element transport from slab to volcanic front at the Mariana arc. J. Geophys. Res. 102, 14991. doi:10.1029/97JB00788

Elliott Tim, 1997. Fractionation of U and Th during mantle melting : a reprise. Chem. Geol. 139, 165–183. doi:http://dx.doi.org/10.1016/S0009-2541(97)00034-X

Ewart, A., Bryan, W.B., GILL, J.B., 1973. Mineralogy and Geochemistry of the Younger Volcanic Islands of Tonga, S.W. Pacific. J. Petrol. 14, 429–465. doi:10.1093/petrology/14.3.429

Feigenson, M.D., Hofmann, A.W., Spera, F.J., 1983. Case studies on the origin of basalt. Contrib. to Mineral. Petrol. 84, 390–405. doi:10.1007/BF01160290

Freymuth, H., Vils, F., Willbold, M., Taylor, R.N., Elliott, T., 2015. Molybdenum mobility and isotopic fractionation during subduction at the Mariana arc. Earth Planet. Sci. Lett. 432, 176–186. doi:10.1016/j.epsl.2015.10.006

Gale, A., Dalton, C.A., Langmuir, C.H., 2013. The mean composition of ocean ridge basalts 14, 489–518. doi:10.1029/2012GC004334

Gribble, R.F., Stern, R.J., Bloomer, S.H., Stüben, D., O'Hearn, T., Newman, S., 1996. MORB mantle and subduction components interact to generate basalts in the southern Mariana Trough back-arc basin. Geochim. Cosmochim. Acta 60, 2153–2166. doi:http://dx.doi.org/10.1016/0016-7037(96)00078-6

Gribble, R.F., Stern, R.J., Newman, S., Bloomer, S.H., O'Hearn, T., 1998. Chemical and Isotopic Composition of Lavas from the Northern Mariana Trough: Implications for Magmagenesis in Back-arc Basins. J. Petrol. 39, 125–154. doi:10.1093/petroj/39.1.125

Hamilton, P.J., O'Nions, R.K., Bridgwater, D., Nutman, A., 1983. Sm-Nd studies of Archaean metasediments and metavolcanics from West Greenland and their implications for the Earth's early history. Earth Planet. Sci. Lett. 62, 263–272. doi:10.1016/0012-821X(83)90089-4

Hermann, J., Spandler, C.J., 2008. Sediment melts at sub-arc depths: An experimental study. J. Petrol. 49, 717–740. doi:10.1093/petrology/egm073

Hochstaedter, A., Gill J., Peters R., Broughton P., Holden P. and Taylor B., 2001. Across-arc geochemical trends in the Izu-Bonin arc: contributions from the subducting slab. Geochemistry Geophys. Geosystems 2, 1525-2027.

Hofmann, A., 1988. Chemical differentiation of the Earth: the relationship between mantle, continental crust, and oceanic crust. Earth Planet. Sci. Lett. 90, 297–314.

Hole, M., Saunders, A., Marriner, G., Tarney, J., 1984. Subduction of Pelagic Sediments - Implications for the Origin of Ce-Anomalous Basalts From the Mariana Islands 141, 453–472. doi:10.1144/gsjgs.141.3.0453

Ishikawa, T., Nakamura, E., 1994. Origin of the slab component in arc lavas from across-arc variation of B and Pb isotopes. Nature 370, 205–208. doi:10.1038/370205a0

Ishikawa, T., Tera, F., 1999. Two isotopically distinct fluid components involved in the Mariana Arc: Evidence from Nb/B ratios and B, Sr, Nd, and Pb isotope systematics. Geology 27, 83–86.

Jakes, P., Gill, J., 1970. Rare earth elements and the island arc tholeiitic series. Earth Planet. Sci. Lett. 9, 17–28. doi:http://dx.doi.org/10.1016/0012-821X(70)90018-X

Johnson, M.C., Plank, T., 1999. Dehydration and melting experiments constrain the fate of subducted sediments. Geochemistry Geophys. Geosystems 1, 1. doi:10.1029/1999GC000014

Karl, S.M., Wandless, G. a, Karpoff, a M., 1992. Sedimentological and geochemical characteristics of Leg 129 siliceous deposits. . Larson R.L., Lancelot Y. al., Proc. ODP, Sci. Results, 129, Coll. Station. TX (Ocean Drill. Program) 129, 31–79.

Karpoff, A.M., 1992. Cenozoic and Mesozoic sediments from the Pigafetta Basin, Leg 129, Sites 800 and 801: mineralogical and geochemical trends of the deposits overlying the oldest oceanic crust. Proc. Ocean Drill. Program, Sci. Results 129, 3–30. doi:doi:10.2973/odp.proc.sr.129.110.1992

Karpoff, A.M., France-Lanord, C., Lothe, F., Karcher, P., 1992. Miocene tuff from Mariana Basin, Leg 129, Site 802: a first deep-sea occurrence of thaumasite. Proc., Sci. results, ODP, Leg 129, old Pacific crust 129, 119–135.

Kelley, K.A., Cottrell, E., 2009. Water and the oxidation state of subduction zone magmas. Science 325, 605–607. doi:https://doi.org/10.1126/science.1174156

Kelley, K.A., Plank, T., Newman, S., Stolper, E.M., Grove, T.L., Parman, S., Hauri, E.H., 2010. Mantle Melting as a Function of Water Content beneath the Mariana Arc. J. Petrol. 51, 1711–1738. doi:10.1093/petrology/egq036

Klemme, S., Prowatke, S., Hametner, K., Günnther, D., 2005. Partitioning of trace elements between rutile and silicate melts: Implications for subduction zones. Geochim. Cosmochim. Acta 69, 2361–2371. doi:10.1016/j.gca.2004.11.015

Kohut, E. and Savov, I. P., 2008. Mantle Heterogeneity in the Southern Mariana Trough Indicated Through B and Sr Isotopic Systematics, Eos Trans. AGU, 89(53), Fall Meet. Suppl. Abstract V31A-2110.

Koppers, A.A.P., Staudigel, H., Pringle, M.S., Wijbrans, J.R., 2003. Short-lived and discontinuous intraplate volcanism in the South Pacific: Hot spots or extensional volcanism? Geochemistry, Geophys. Geosystems 4, n/a--n/a. doi:10.1029/2003GC000533

Larson, R.L., Lancelot, Y., 1992. proceding Ocean Drilling Program scientific results, 129. doi:doi:10.2973/odp.proc.sr.129.

Lawrence, M. G., Greig, A., Collerson, K. D., & Kamber, B. S. (2006). Rare earth element and yttrium variability in South East Queensland waterways. *Aquatic Geochemistry*, *12*(1), 39-72.

Longerich, H.P., 1993. Oxychlorine ions in inductively coupled plasma mass spectrometry: Effect of chlorine speciation as Cl- and ClO4\n-. J. Anal. At. Spectrom. 8, 439–444.

Luhr, J.F. Carmichael, I.S.E., 1980. The Colima volcanic complex, Mexico. I: post-caldera andesites from Volcan Colima. Contributions to Mineralogy and Petrology 71: 343-372.

Makishima, A., Masuda, A., 1994. Ce isotope ratios of N-type MORB. Chem. Geol. 118, 1–8.

Makishima, A., Shimizu, H., Masuda, A., 1987. Precise Measurement of Cerium and Lanthanum isotope ratios. mass Spectrom. 35.

Martindale, M., Skora, S., Pickles, J., Elliott, T., Blundy, J., Avanzinelli, R., 2013. High pressure phase relations of subducted volcaniclastic sediments from the west pacific and their implications for the geochemistry of Mariana arc magmas. Chem. Geol. 342, 94–109. doi:10.1016/j.chemgeo.2013.01.015

McDonough, W.., Sun, S. -s., 1995. The composition of the Earth. Chem. Geol. 120, 223–253.

McKenzie, D., O'Nions, R.K., 1991. Partial Melt Distributions from Inversion of Rare Earth Element Concentrations. J. Petrol. 32, 1021–1091. doi:10.1093/petrology/32.5.1021

Meijer, A., 1976. Pb and Sr isotopic data bearing on the origin of volcanic rocks from the Mariana island-arc system. Geol. Soc. Am. Bull. 87, 1358–1369. doi:10.1130/0016-7606(1976)87<1358:PASIDB>2.0.CO;2

Meijer, A., Reagan, M., 1981. Petrology and geochemistry of the island of Sarigan in the Mariana Arc; calc-alkaline volcanism in an oceanic setting. Contrib. to Mineral. Petrol. 77, 337–354.

Moiroud, M., Pucéat, E., Donnadieu, Y., Bayon, G., Guiraud, M., Voigt, S., Deconinck, J.-F., Monna, F., 2015. Evolution of neodymium isotopic signature of seawater during the Late Cretaceous: Implications for intermediate and deep circulation. Gondwana Res. doi:http://dx.doi.org/10.1016/j.gr.2015.08.005

Moriguti, T., Nakamura, E., 1998. Across-arc variation of Li isotopes in lavas and implications for crust/mantle recycling at subduction zones. Earth Planet. Sci. Lett. 163, 167–174. doi:http://dx.doi.org/10.1016/S0012-821X(98)00184-8

Papike, J.J., Karner, J.M., Shearer, C.K., 2005. Comparative planetary mineralogy : Valence state partitioning of Cr , Fe , Ti , and V among crystallographic sites in olivine , pyroxene , and spinel from planetary basalts. Am. Mineral. 90, 277–290. doi:10.2138/am.2005.1779

Parkinson, I.J., Arculus, R.J., 1999. The redox state of subduction zones: Insights from arc peridotites. Chem. Geol. 160, 409–423.

Pearce, J. a., Stern, R.J., Bloomer, S.H., Fryer, P., 2005. Geochemical mapping of the Mariana arc-basin system: Implications for the nature and distribution of subduction components. Geochemistry, Geophys. Geosystems 6. doi:10.1029/2004GC000895

Peate, D. W., Pearce, J. A., Hawkesworth, C. J., Colley,H., Edwards C., M., H., Hirose K. 1997. Geochemical variations in Vanuatu arc lavas: the role of subducted material and a variable mantle wedge composition. J. Petrol., 10, 1331-1358.

Picard, S., Lécuyer, C., Barrat, J.A., Garcia, J.P., Dromart, G., Sheppard, S.M.F., 2002. Rare earth element contents of Jurassic fish and reptile teeth and their potential relation to seawater composition (Anglo-Paris Basin, France and England). Chem. Geol. 186, 1–16. doi:10.1016/S0009-2541(01)00424-7

Pin, C., Santos Zalduegui lt, J.F., 1997. Sequential separation of light rare-earth elements , thorium and uranium by miniaturized extraction chromatography : Application to isotopic analyses of silicate rocks. Anal. Chim. Acta 339, 79–89.

Plank, T., 2013. The Chemical Composition of Subducting Sediments, 2nd ed, Treatise on Geochemistry: Second Edition. Elsevier Ltd. doi:10.1016/B978-0-08-095975-7.00319-3

Plank, T., Cooper, L.B., Manning, C.E., 2009. Emerging geothermometers for estimating slab surface temperatures. Nat. Geosci. 2, 611–615. doi:10.1038/ngeo614

Plank, T., Langmuir, C.H., 1998. The chemical composition of subducting sediment and its consequences for the crust and mantle. Chem. Geol. 145, 325–394. doi:10.1016/S0009-2541(97)00150-2

Pourmand, A., Dauphas, N., Ireland, T.J., 2012. A novel extraction chromatography and MC-ICP-MS technique for rapid analysis of REE, Sc and Y: Revising CI-chondrite and Post-Archean Australian Shale (PAAS) abundances. Chem. Geol. 291, 38–54. doi:10.1016/j.chemgeo.2011.08.011

Prytulak, J., Nielsen, S.G., Ionov, D.A., Halliday, A.N., Harvey, J., Kelley, K.A., Niu, Y.L., Peate, D.W., Shimizu, K., Sims, K.W.W., 2013a. The stable vanadium isotope composition of the mantle and mafic lavas. Earth Planet. Sci. Lett. 365, 177–189. doi:10.1016/j.epsl.2013.01.010

Prytulak, J., Nielsen, S.G., Plank, T., Barker, M., Elliott, T., 2013b. Assessing the utility of thallium and thallium isotopes for tracing subduction zone inputs to the Mariana arc. Chem. Geol. 345, 139–149. doi:10.1016/j.chemgeo.2013.03.003

Prytulak, J., Sossi, P.A., Halliday, A.N., Plank, T., Savage, P.S., Woodhead, J.D., 2017. Stable vanadium isotopes as a redox proxy in magmatic systems ? geochemical Perspect. Lett. 3, 75–84. doi:10.7185/geochemlet.1708

Ribeiro, J.M., Stern, R.J., Kelley, K.A., Shaw, A.M., Martinez, F., Ohara, Y., 2015. Composition of the slab-derived fluids released beneath the Mariana forearc: Evidence for shallow dehydration of the subducting plate. Earth Planet. Sci. Lett. 418, 136–148. doi:10.1016/j.epsl.2015.02.018

Rollinson, H., 1993. Using geochemical data: evaluation, presentation, interpretation, longman gr. ed.

Rubatto, D., Hermann, J., 2003. Zircon formation during fluid circulation in eclogites (Monviso, Western Alps): Implications for Zr and Hf budget in subduction zones. Geochim. Cosmochim. Acta 67, 2173–2187. doi:10.1016/S0016-7037(02)01321-2

Salimullah, A.R.M., 1992. Volcaniclastic facies and sequences, Leg 129. Proc. Ocean Drill. Program, Sci. Results 129. doi:10.1029/138GM10

Salters, V.J.M., Stracke, A., 2004. Composition of the depleted mantle. Geochemistry, Geophys. Geosystems 5. doi:10.1029/2003GC000597

Savage, P.S., Georg, R.B., Armytage, R.M.G., Williams, H. M., Halliday, A.N., 2010. Silicon isotope homogeneity in the mantle. Earth Planet. Sci. Lett., *295*, 139-146.

Savov, I.P., Ryan, J.G., D'Antonio, M., Fryer, P., 2007. Shallow slab fluid release across and along the Mariana arc-basin system: Insights from geochemistry of serpentinized peridotites from the Mariana fore arc. J. Geophys. Res. Solid Earth 112. doi:10.1029/2006JB004749

Savov, I.P., Ryan, J.G., D'Antonio, M., Kelley, K., Mattie, P., 2005. Geochemistry of serpentinized peridotites from the Mariana Forearc Conical Seamount, ODP Leg 125: Implications for the elemental recycling at subduction zones. Geochemistry, Geophys. Geosystems 6, 1–24. doi:10.1029/2004GC000777

Schiano, P., Birck, J., Alegre, C.J., 1997. Osmium-strontium-neodymium-lead 150, 363–379.

Schiano, P., Monzier, M., Eissen, J.P., Martin, H., Koga, K.T., 2010. Simple mixing as the major control of the evolution of volcanic suites in the Ecuadorian Andes. Contrib. to Mineral. Petrol. 160, 297–312. doi:10.1007/s00410-009-0478-2

Schreiber, H.D., 1987. An Electrochemical Series of Redox Couples in Silicate Melts: a review and applications to geochemistry. J. Geophys. Res. 92, 9225–9232. doi:10.1029/JB092iB09p09225

Schreiber, H.D., Lauer, H. V, Thanyasiri, T., 1980. The redox state of cerium in basaltic magmas: an experimental study of iron-cerium interactions in silicate melts. Geochim. Cosmochim. Acta 44, 1599–1612. doi:http://dx.doi.org/10.1016/0016-7037(80)90120-9

Schuth S., Munker C., Konig S., Qopoto C., Basi S., Garde-Schonberg D and Ballaus C., 2009. Petrogenesis of lavas along the Solomon Island ARc, SW Pacific: Coupling of compositional variations and subduction Zone Geometry. J. Petrol. 50, 781-811.

Seno, T., 1977. The instantaneous rotation vector of the Philippine Sea plate relative to the Eurasian plate. Tectonophysics 42, 209–226.

Shimizu, H., Sawatari, H., Kawata, Y., Dunkley, P.N., Masuda, A., 1992. Ce and Nd isotope geochemistry on island arc volcanic rocks with negative Ce anomaly: existence of sources with concave REE patterns in the mantle beneath the Solomon and Bonin island arcs. Contrib. to Mineral. Petrol. 110, 242–252. doi:10.1007/BF00310741

Skora, S., Blundy, J., 2012. Monazite solubility in hydrous silicic melts at high pressure conditions relevant to subduction zone metamorphism. Earth Planet. Sci. Lett. 321–322, 104–114. doi:10.1016/j.epsl.2012.01.002

Skora, S., Freymuth, H., Blundy, J., Elliott, T., Guillong, M., 2017. An experimental study of the behaviour of cerium / molybdenum ratios during subduction : Implications for tracing the slab component in the Lesser Antilles and Mariana Arc. Geochim. Cosmochim. Acta 212, 133–155. doi:10.1016/j.gca.2017.05.025

Smythe, D.J., Brenan, J.M., 2016. Magmatic oxygen fugacity estimated using zircon-melt partitioning of cerium. Earth Planet. Sci. Lett. 453, 260–266. doi:10.1016/j.epsl.2016.08.013

Smythe, D.J., Brenan, J.M., 2015. Cerium Oxidation State in Silicate Melts: Combined fO2, Temperature and Compositional Effects. Geochim. Cosmochim. Acta. doi:http://dx.doi.org/10.1016/j.gca.2015.07.016

Snyder, G.T., Savov, I. P., Muramatsu, Y., 2004. Iodine and boron in Mariana serpentine mud volcanoes (ODP 125 and 195): Implications for forearc processes and subduction recycling, In Shinohara, M., Salisbury, M.H., and Richter, C. (Eds.), Proc. ODP, Sci. Results, 195

Stern, R.J., Fouch, M.J., Klemperer, S.L., 2003. An overview of the Izu-Bonin-Mariana subduction factory. Insid. subduction Fact., Geophysical Monograph. doi:10.1029/138GM10

Stolper, E., Newman, S., 1994. The role of water in the petrogenesis of Mariana trough magmas. Earth Planet. Sci. Lett. 121, 293–325. doi:10.1016/0012-821X(94)90074-4

Straub, S.M., 2003. The evolution of the Izu Bonin - Mariana volcanic arcs (NW Pacific) in terms of major element chemistry. Geochemistry, Geophys. Geosystems 4, 1–33. doi:10.1029/2002GC000357

Syracuse, E.M., Abers, G.A., 2006. Global compilation of variations in slab depth beneath arc volcanoes and implications. Geochemistry, Geophys. Geosystems 7, n/a--n/a. doi:10.1029/2005GC001045

Syracuse, E.M., van Keken, P.E., Abers, G.A., 2010. The global range of subduction zone thermal models. Phys. Earth Planet. Inter. 183, 73–90. doi:10.1016/j.pepi.2010.02.004

Tanaka, T., Togashi, S., Kamioka, H., Amakawa, H., Kagami, H., Hamamoto, T., Yuhara, M., Orihashi, Y., Yoneda, S., Shimizu, H., Kunimaru, T., Takahashi, K., Yanagi, T., Nakano, T., Fujimaki, H., Shinjo, R., Asahara, Y., Tanimizu, M., Dragusanu, C., 2000. JNdi-1: a neodymium isotopic reference in consistency with LaJolla neodymium, Chemical Geology. doi:10.1016/S0009-2541(00)00198-4

Tanimizu, M., 2000. Geophysical determination of the 138La β- decay constant. Phys. Rev. 62, 140–143.

Taylor, B., Martinez, F., 2003. Back-arc basin basalt systematics. Earth Planet. Sci. Lett. 210, 481–497. doi:10.1016/S0012-821X(03)00167-5

Tollstrup, D.L., Gill, J.B., 2005. Hafnium systematics of the Mariana arc: Evidence for sediment melt and residual phases. Geology 33, 737–740. doi:10.1130/G21639.1

Trail, D., Watson, E.B., Tailby, N.D., 2011. The oxidation state of Hadean magmas and implications for early Earth's atmosphere. Nature 480, 79-U238. doi:10.1038/nature10655

Tsay, A., Zajacz, Z., Ulmer, P., Sanchez-Valle, C., 2017. Mobility of major and trace elements in the eclogite-fluid system and element fluxes upon slab dehydration. Geochim. Cosmochim. Acta 198, 70–91. doi:10.1016/j.gca.2016.10.038

Vervoort, J.D., Plank, T., Prytulak, J., 2011a. The Hf-Nd isotopic composition of marine sediments. Geochim. Cosmochim. Acta 75, 5903–5926. doi:10.1016/j.gca.2011.07.046

Vervoort, J.D., Plank, T., Prytulak, J., 2011b. The Hf–Nd isotopic composition of marine sediments. Geochim. Cosmochim. Acta 75, 5903–5926. doi:10.1016/j.gca.2011.07.046

Volpe, A.M., Douglas Macdougall, J., Hawkins, J.W., 1987. Mariana Trough basalts (MTB): trace element and SrNd isotopic evidence for mixing between MORB-like and Arc-like melts. Earth Planet. Sci. Lett. 82, 241–254. doi:10.1016/0012-821X(87)90199-3

Voegelin, A. R., Pettke, T., Greber, N. D., von Niederhäusern, B., & Nägler, T. F., 2014. Magma differentiation fractionates Mo isotope ratios: evidence from the Kos Plateau Tuff (Aegean Arc). Lithos, 190, 440-448.

von Huene, R., Scholl, D.W., 1991. Observations at convergent margins concerning sediment subduction, subduction erosion, and the growth of continental crust. Rev. Geophys. 29, 279. doi:10.1029/91RG00969

Vroon, P.Z., Bergen, M.J. van, Klaver, G.J., White, W.M., 1995. Strontium, neodymium, and lead isotopic and trace-element signatures of the {East} indonesian sediments: provenance and implications for banda arc magma genesis. Geochim. Cosmochim. Acta 59, 2573–2598. doi:http://dx.doi.org/10.1016/0016-7037(95)00151-4

Wade, J. a., Plank, T., Stern, R.J., Tollstrup, D.L., Gill, J.B., O'Leary, J.C., Eiler, J.M., Moore, R.B., Woodhead, J.D., Trusdell, F., Fischer, T.P., Hilton, D.R., 2005. The May 2003 eruption of Anatahan volcano, Mariana Islands: Geochemical evolution of a silicic island-arc volcano. J. Volcanol. Geotherm. Res. 146, 139–170. doi:10.1016/j.jvolgeores.2004.11.035

Williams, H.M., Prytulak, J., Woodhead, J.D., Kelley, K.A., Brounce, M., Plank, T., 2018. Interplay of crystal fractionation, sulfide saturation and oxygen fugacity on the iron isotope composition of arc lavas: an example from the Marianas. Geochim. Cosmochim. Acta, *226*, 224-243.

White, W.M., Dupré, B., 1986. Sediment subduction and magma genesis in the Lesser Antilles: isotopic and trace element constraints. J. Geophys. Res. Solid Earth 91, 5927–5941. doi:10.1029/JB091iB06p05927

White, W.M., Patchett, J., 1984. HfNdSr isotopes and incompatible element abundances in island arcs: implications for magma origins and crust-mantle evolution. Earth Planet. Sci. Lett. 67, 167–185. doi:10.1016/0012-821X(84)90112-2

Willbold M. (2007) Determination of Ce isotopes by TIMS and MC-ICPMS and initiation of a new, homogeneous Ce isotopic reference material. J. Anal. At. Spectrom. 22(22), 1364–1372. doi:10.1039/b705306a

Willig, M., and Stracke, A., 2018) Accurate and precise measurement of Ce isotope ratios by thermal ionization mass spectrometry (TIMS). *Chemical Geology*, *476*, 119-129.

Woodhead, J., Eggins, S., Gamble, J., 1993. High field strength and transition element systematics in island arc and back-arc basin basalts: Evidence for multi-phase melt extraction and a depleted mantle wedge. Earth Planet. Sci. Lett. 114, 491–504. doi:10.1016/0012-821X(93)90078-N

Woodhead, J., Stern, R.J., Pearce, J., Hergt, J., Vervoort, J., 2012. Hf-Nd isotope variation in Mariana Trough basalts: The importance of “ambient mantle” in the interpretation of subduction zone magmas. Geology 40, 539–542. doi:10.1130/G32963.1

Woodhead, J.D., 1989. Geochemistry of the Mariana arc (western Pacific): Source composition and processes. Chem. Geol. 76, 1–24. doi:10.1016/0009-2541(89)90124-1

Woodhead, J.D., 1988. The origin of geochemical variations in Mariana lavas: A general model for petrogenesis in intra-oceanic island arcs? J. Petrol. 29, 805–830. doi:10.1093/petrology/29.4.805

Woodhead, J.D., Fraser, D.G., 1985. Pb, Sr and 10Be isotopic studies of volcanic rocks from the Northern Mariana Islands. Implications for magma genesis and crustal recycling in the Western Pacific. Geochim. Cosmochim. Acta 49, 1925–1930. doi:http://dx.doi.org/10.1016/0016-7037(85)90087-0

Workman, R.K., Hart, S.R., 2005. Major and trace element composition of the depleted MORB mantle (DMM). Earth Planet. Sci. Lett. 231, 53–72. doi:10.1016/j.epsl.2004.12.005

Figure captions

Figure 1: Bathymetric map of the Mariana arc showing the location of the samples analyzed in this study. Blue triangles: arc volcanoes; red circles: Mariana Trough (backarc) basalts; and white squares: ODP drilling sediment sites from Leg 129 (800, 801 and 802). The basemap is from GeoMapApp (www.geomapapp.org).

Figure 2: Stratigraphic log of site 801 from ODP Leg 129 and the associated Ce anomaly (Ce/Ce*) in function of depth (meters below sea level). Ce anomalies are calculated from data published in Karl et al. (1992) and Plank and Langmuir (1998) measured by INAA and ICPMS, respectively. The red arrows indicate the provenance of each studied sedimentary sample (Karl et al., 1992; Karpof, 1992; Salimullah, 1992).

Figure 3: Ce/Ce* of studied lava samples from Mariana arc relative to (A) ε_{Nd} and (B) ε_{Ce}. Epsilon Ce values correspond to the weighted mean value when measurements have been duplicated. The error bar at the top of the diagram corresponds to the 2S.D. value determined on repeated standard measurements (40 ppm for ε_{Ce} and 9 ppm for ε_{Nd}). Deep blue triangle = Guguan; light blue triangle = Alamagan; orange triangle = Pagan; black triangle= Agrigan; grey triangle = Sagrigan; green triangle = Ascuncion; white triangle = Uracas.

Figure 4: REE patterns of the three studied Mariana Trough basalts normalized to CI-chondrite (McDonough and Sun, 1995). The N-MORB from Hofmann (1988) is shown for comparison (black line). Sample D68-2-1 is depleted in Light REE and follows the same pattern as N-MORB, whereas C7 and D3-2-1 are enriched in LREE.

Figure 5: A) ε_{Ce} vs ε_{Nd} values for MTB (red diamonds), Pacific MORB (orange circles), Mariana arc samples (blue triangles) and biosiliceous sediments (green squares). The 2SD for ε_{Ce} and ε_{Nd} illustrates the external reproducibility on repeated measurements of AMES and JNdi-1 standards. The two curves correspond to binary mixing between the Mariana Trough basalt D68-2-1 and components derived from biosiliceous sediments D68-801B33R

and D68-801A17R that show the most extreme ε_{Ce} values. The white stars indicate the sedimentary proportions needed to explain the Ce and Nd isotopic compositions of the volcanic arc samples. Similar results are obtained using a «mean» sedimentary component (supplementary information). B) Evolution of the modeled Ce/Ce* with respect to the sedimentary proportions determined using the binary mixing models in Figure 5A. The white dots corresponds to Ce/Ce* calculated for 2.5% to 8% of sedimentary products at the lava source. The modeled Ce anomalies can be compared with the Ce/Ce* range in the Mariana arc samples represented in the right part of the figure B. Input parameters of the models are given in Table 3.

Figure 6 A) ε_{Ce} vs ε_{Nd} values for MTB (red diamonds), Pacific MORB (orange circles), Mariana arc samples (blue triangles) and volcaniclastic sediments (purple squares). The 2SD in ε_{Ce} and ε_{Nd} illustrates the external reproducibility on repeated measurements of AMES and JNdi-1 standards. The two curves correspond to binary mixing between the Mariana Trough basalt D68-2-1 and components derived from volcaniclastic sediments (samples 801B-8R3 and 801B-7R which $^{138}Ce/^{142}Ce$ compositions are the two most extreme) as enriched end-members. The white stars indicate the sedimentary proportions allowing to reproduce the Ce and Nd isotopic compositions of the arc lavas with melt products from volcaniclastic sediments in their source. Similar results are obtained using a «mean» sedimentary component (supplementary information). B) Evolution of the modeled Ce/Ce* with respect to the sedimentary proportions. The white dots correspond to Ce/Ce* calculated for 0.75% to 2.75% of sedimentary products at the lava source. The modeled Ce anomalies can be compared with the Ce/Ce* range in the Mariana arc samples represented in the right part of the figure B. Input parameters of the models are given in Table 3.

Figure 7: Dispersion of Ce anomalies (Ce/Ce*) in arc samples from many different subduction zones. All data are from the Georoc database (convergent margins data, http://**georoc**. mpch-mainz. gwdg.de). Ce/Ce* are calculated using $Ce/Ce^* = Ce_N / (La_N^{0.5} \times Pr_N^{0.5})$.

Figure 8: Evolution of Ce/Ce* anomaly during (A) batch melting and (B) fractional crystallization. The ΔCe/Ce* represents the Ce/Ce* of the melt subtracted to the Ce/Ce* of the initial solid/melt (100% of melting in A and 100% of liquid in B). To produce diagram A, we considered 2 modal compositions: a garnet peridotite (55% ol, 25% opx, 11% cpx, 9% grt, black line) and a spinel-garnet peridotite (55% ol, 25% opx, 11% cpx, 6% grt, 3% sp; grey line). We also used the sedimentary proportions involved in the magma genesis defined from Ce-Nd isotopes: 2% of melt extracted from volcaniclastic sediments (Mariana) and 5% fluids coming from the partial melting of the GLOSS-II reservoir (Martinique). The fluid composition was calculated by applying the bulk solid/fluid partition coefficients measured from the experiments carried out by Martindale et al. (2013) for Mariana and by Johnson and Plank (1999) for Lesser Antilles. Light REE concentrations of the mantle source are those proposed by Salters and Stracke (2004) for the depleted mantle. The bulk partition coefficients (D) of the garnet-spinel peridotite are K_D values of McKenzie and O'Nions (1991). ΔCe/Ce* values are identical whatever the sediment proportions and the nature of the sediments showing that only the mineralogy of the mantle wedge changes the cerium anomaly of the produced melt. In diagram B, the blue line corresponds to the Mariana and the red field to Martinique. The crystallizing mineral assemblage is 48.6% plagioclase, 35.9% clinopyroxene, 1.1% orthopyroxene, 7.3% olivine and 7.1% magnetite (Table 5 in Dixon and Batiza, 1979) for Mariana, whereas a range of compositions has been tested for Martinique andesites using the propositions made in Labanieh et al. (2012): 45-50% plagioclase, 30-45% hornblende, 7-10% orthopyroxene, 3-5% clinopyroxene, 0-5% garnet. The initial magmas are similar to those produced by 10% of partial melting in figure A.

Figure 9: Th/Nd vs Nd for (A) Mariana lavas and (B) Martinique lavas. For the Mariana samples, Th and Nd concentrations are from Elliott et al. (1997) and from this study, respectively. Nd and Th concentrations for Martinique lavas are from Labanieh et al. (2012). The box represents a schematic C^H/C^M versus C^H diagram, where C^H and C^M are the concentrations of a highly incompatible element and of a moderately incompatible one (Schiano et al., 2010). A fit forming a near-horizontal line indicates a fractional crystallization

process whereas a positive straight line fit indicates a partial melting process (Allègre and Minster, 1978; Feigenson et al., 1983).

Figure 10: Compilation of ε_{Ce} vs ε_{Nd} data for samples from arc setting including lavas and sediments and mid-ocean ridge basalts. Salomon and Bonin island data are from Shimizu et al. (1992) and $^{138}Ce/^{142}Ce$ ratios are normalized using JMC-304 data (Bellot et al., 2015; Shimizu et al., 1992). Martinique lavas, sediments from DSDP site 144 and a few MORBs are from Bellot et al., (2015). MORB data from Makishima and Masuda (1994) have $^{138}Ce/^{142}Ce$ ratios normalized with BCR-1 and BCR-2.

Figure 11: (A) ε_{Nd} vs Ce/Ce* and (B) ε_{Ce} vs Ce/Ce* for arc settings volcanic rocks. Data from this study and literatures values (Martinique in Bellot et al., 2015 and Labanieh et al., 2010, 2012; Bonin and Salomon from Shimizu et al., 1992). The Ce/Ce* is determined by logarithmic interpolation of La and Pr.

Table captions

Table1: SiO_2 (wt %) and Rare Earth Element concentrations (ppm) for Mariana lavas, sediments from ODP sites 801 and 802, Mariana Trough Basalts and Pacific MORB. All SiO_2 data are from literature (Bézos and Humler, 2005; Elliott et al., 1997; Karl et al., 1992; Karpof, 1992; Karpoff et al., 1992; Pearce et al., 2005; Schiano et al., 1997; Vervoort et al., 2011). REE data were measured in this study by Inductively Coupled Plasma Mass Spectrometer (ICP-MS; quadrupole Agilent 7500) for the following samples: Mariana lavas, 4 of the sediments (802A-19R and 802A-43R, 801B-12R and 801B-7R), Mariana Trough Basalts and Searise 1 DR05 MORB. The analytical precision obtained on 4 repeated measurements of the BIR standard (2SD) varies for each element and is between 0.74% (Nd) to 4.06% (Eu). All the other REE data (sediments from sites 800 and 801, Cyana CY82 and Clipperton DR01 MORB), in italic font, are from the literature. Sediments from ODP sites 801A and 801B are

from Vervoort et al. (2011); two of the Pacific MORB's REE concentrations are from Gale et al. (2013).

Table 2: Results of $^{138}Ce/^{142}Ce$ and $^{143}Nd/^{144}Nd$ isotopic ratios for Mariana arc samples, sediments from ODP 801 and 802, Mariana Trough Basalts and Pacific MORB. The number of the analytical session is given. Some samples have been measured two or three times during the same analytical session (except for D68-2-1 which was in two different sessions). In these cases, the weighted mean value of both run (or all) is considered. (BS) is for biosiliceous sediments and (Volc) for volcaniclastic turbidites. The internal errors are 2s.e (2 times the standard deviation divided by √N where N is the number of cycles). The $^{138}Ce/^{142}Ce$ and $^{143}Nd/^{144}Nd$ ratios are also expressed in ε-notations normalized to CHUR values of 0.0225654 (Bellot et al., 2015) and 0.512630 (Bouvier et al., 2008), respectively.

$\varepsilon = ((^{138}Ce/^{142}Ce_{sample}/^{138}Ce/^{142}Ce_{CHUR}-1)\times 10{,}000)$; $((^{143}Nd/^{144}Nd_{sample}/^{143}Nd/^{144}Nd_{CHUR}-1)\times 10{,}000)$;

Table 3: Input parameters used to calculate the mixing curves presented in Figures 7, 8 and 9. For the depleted end-member the concentrations are those of the DMM published by Salters and Stracke (2004) with a modified La concentration (from 0.234 to 0.265, see text). The concentrations of the two enriched end-members are those of the average sediments multiplied by the enrichment factors defined from experimental studies (Johnson and Plank (1999) for biosiliceous sediments, and from Martindale et al. (2013) for volcaniclastic ones. The ε_{Ce} and ε_{Nd} of each end-member are those measured in the samples. The ε_{Ce} and ε_{Nd} of the depleted end-member are from D68-2-1 Mariana Trough Basalt. Ce/Ce* corresponds to logarithmic calculations between La and Pr.

[a] The enrichment factor is the ratio of element concentration in fluids over element concentration in the solid starting bulk: $C_{fluid}/C_{starting\ bulk}$.

Figure

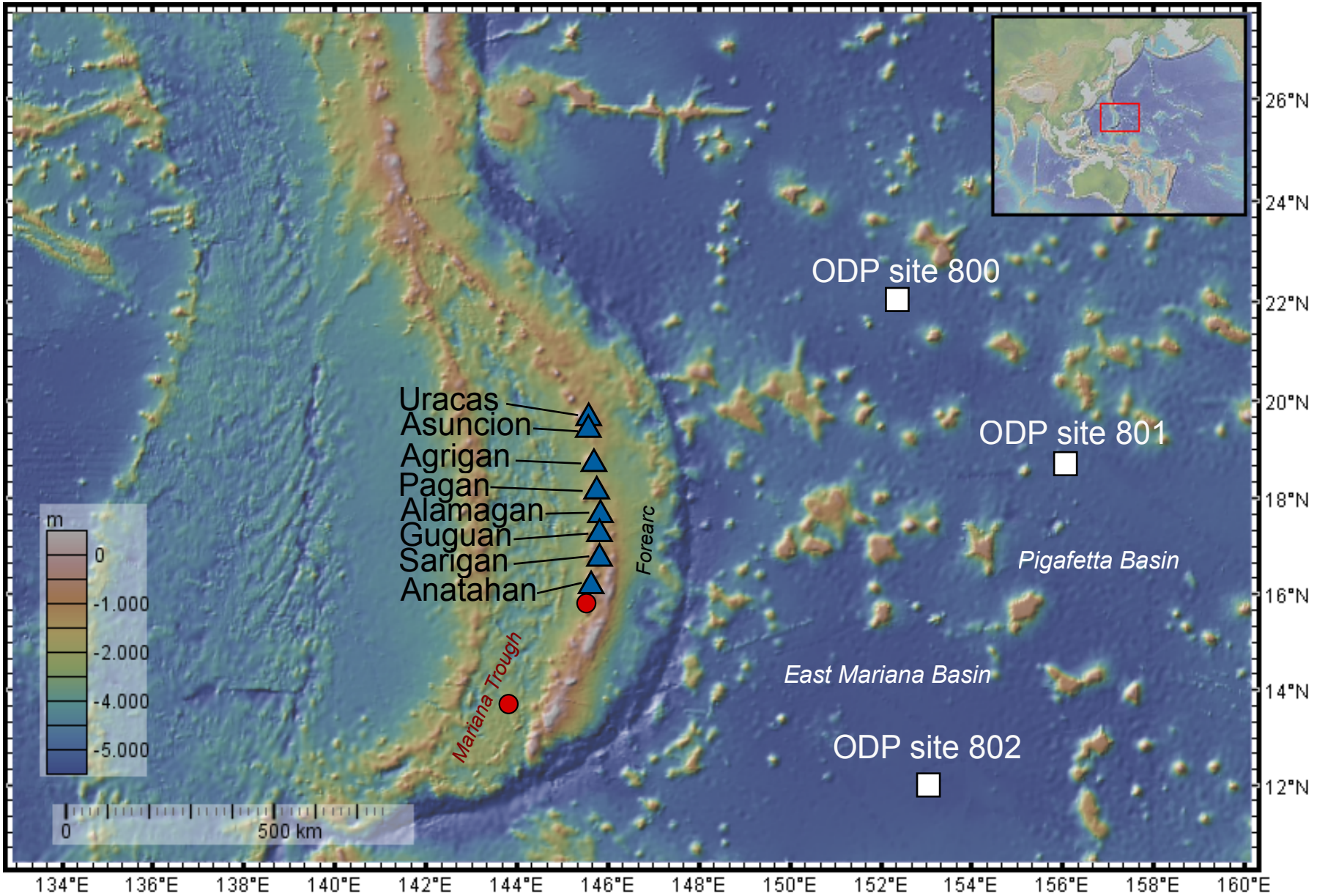

Figure 1 Bellot et al.

Figure

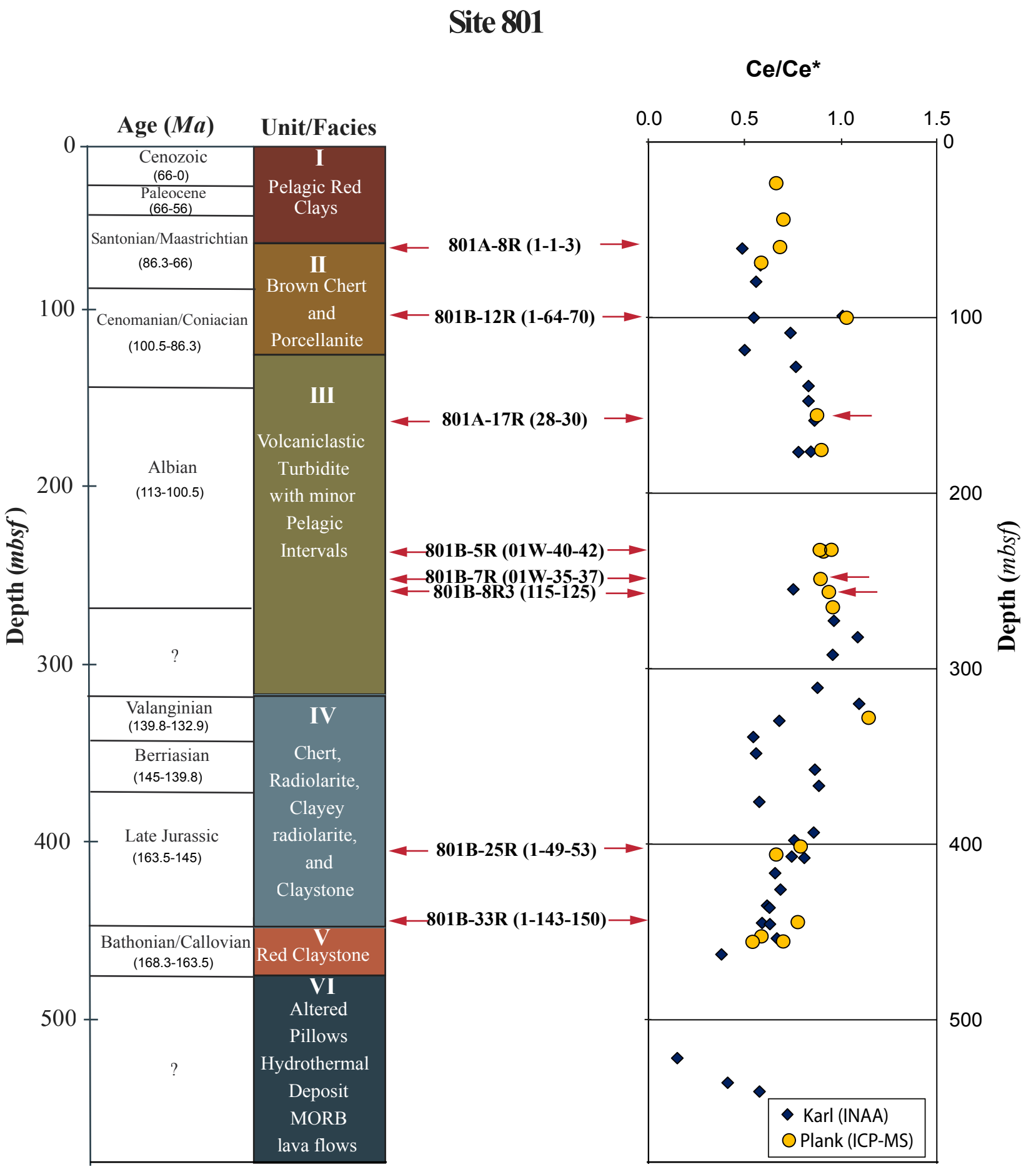

Figure 2 Bellot et al.

Figure

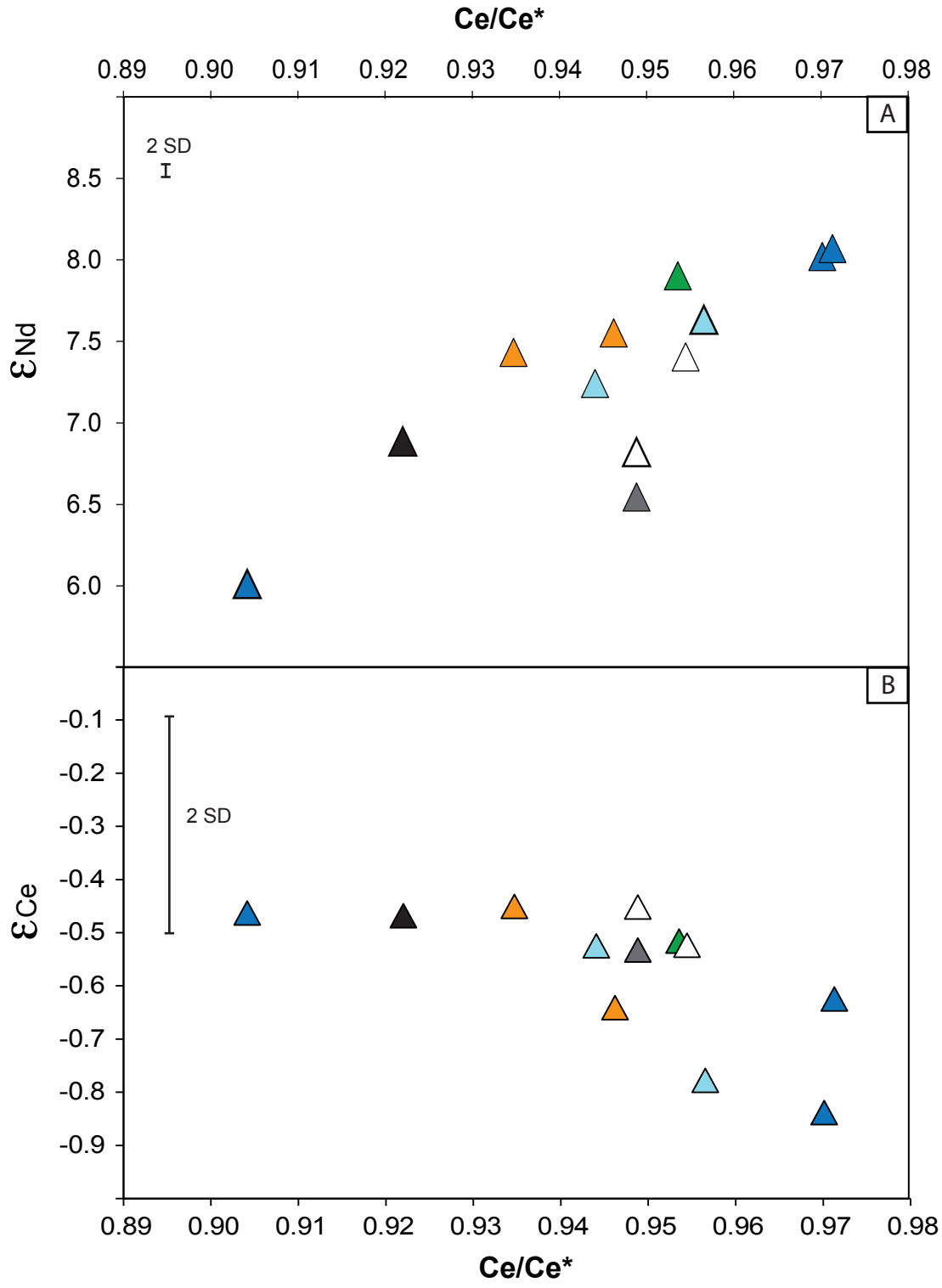

Figure 3. Bellot et al.

Figure

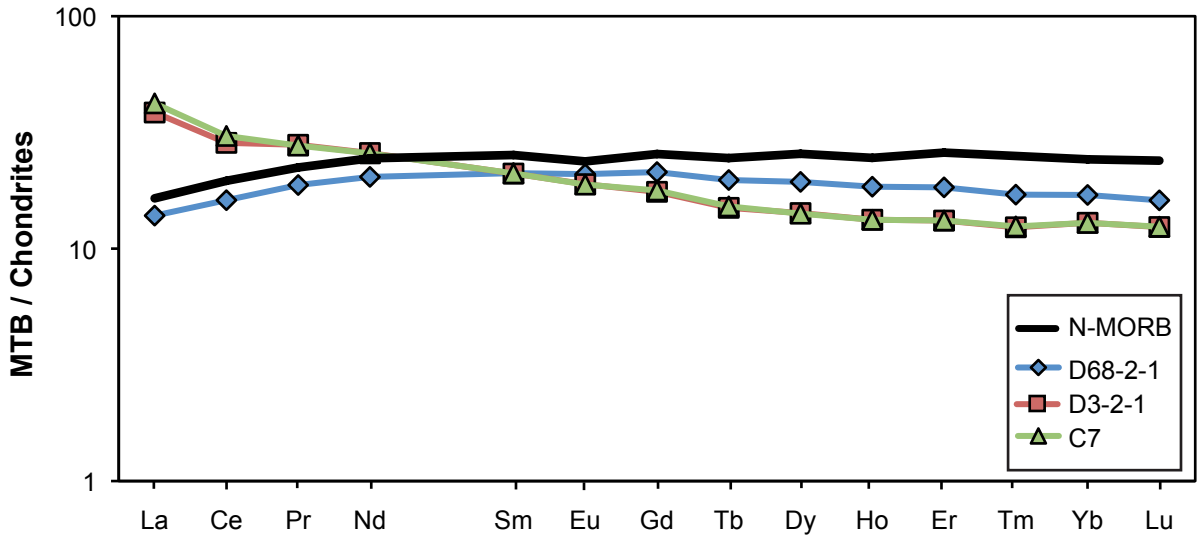

Figure 4. Bellot et al.

Figure

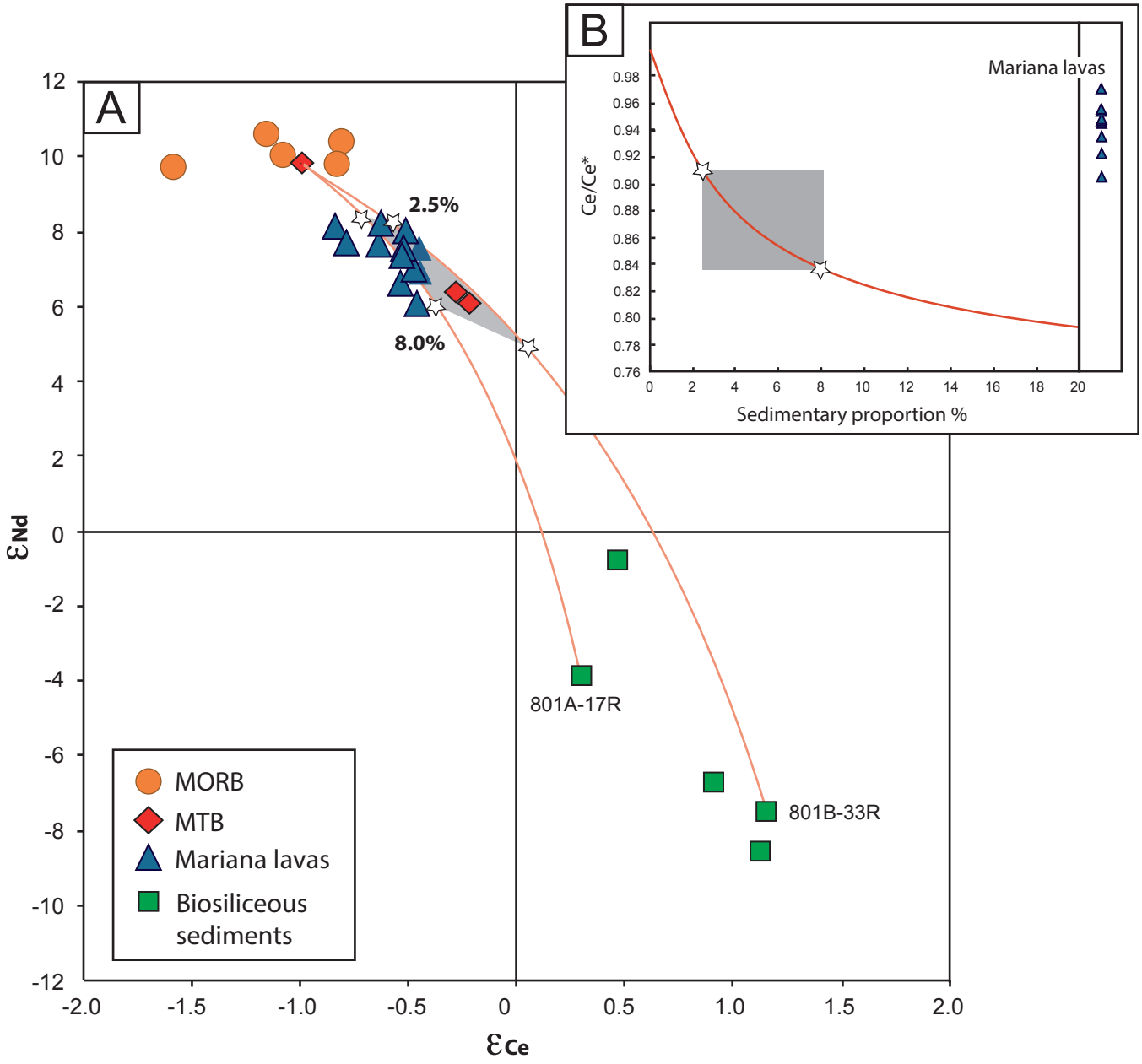

Figure 5. Bellot et al.

Figure

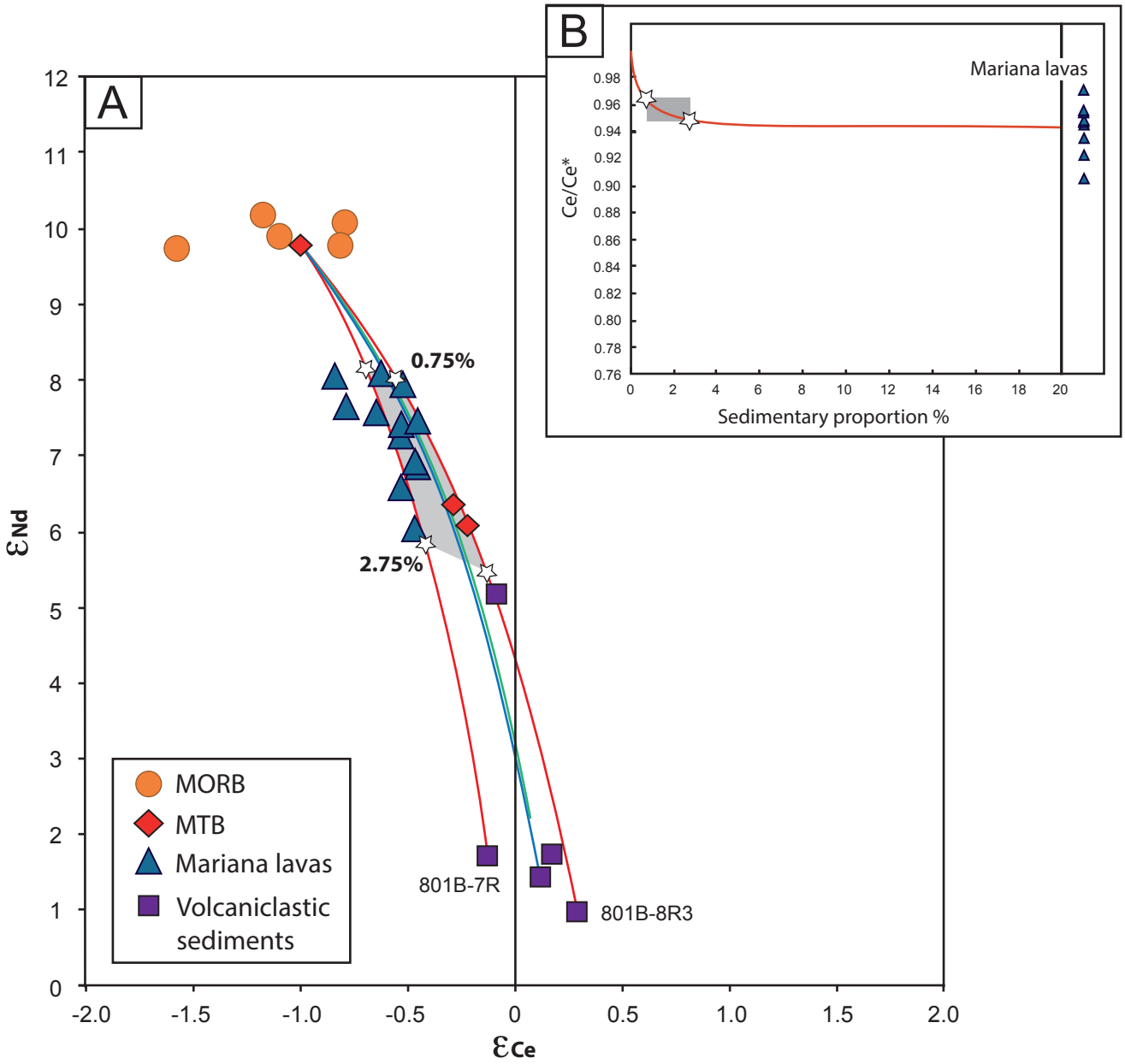

Figure 6. Bellot et al.

Figure

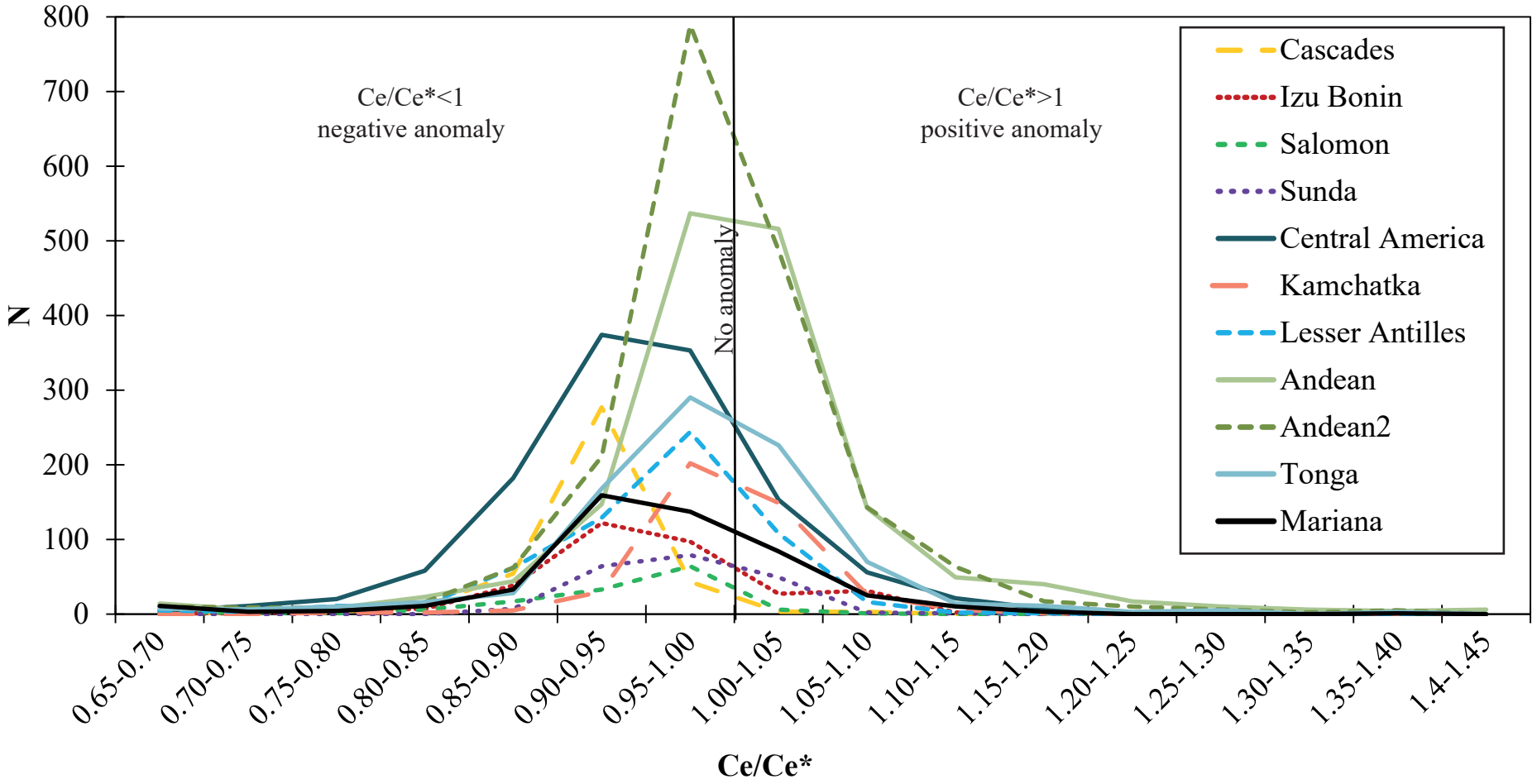

Figure 7 Bellot et al.

Figure

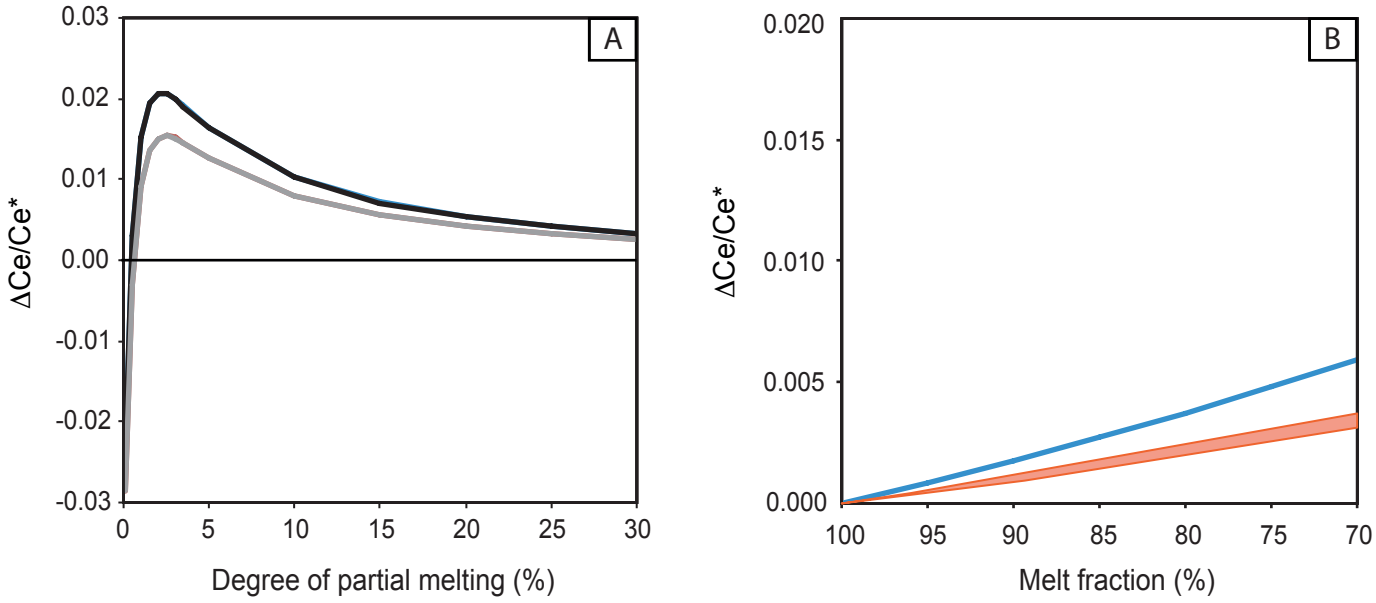

Figure 8. Bellot et al.

Figure

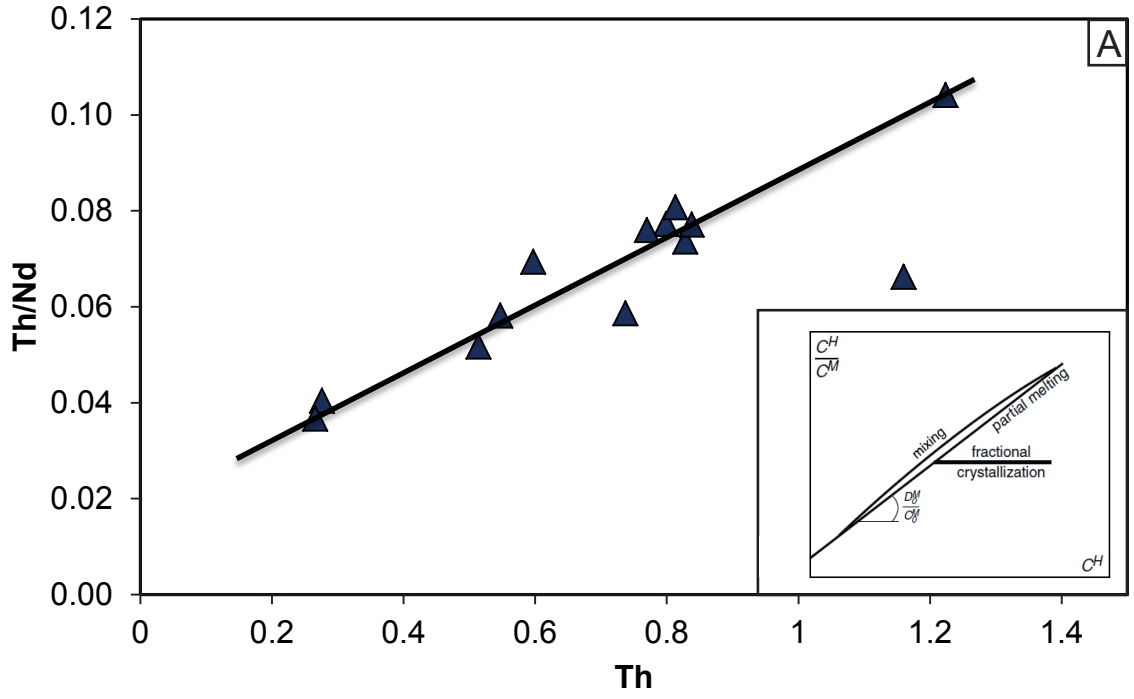

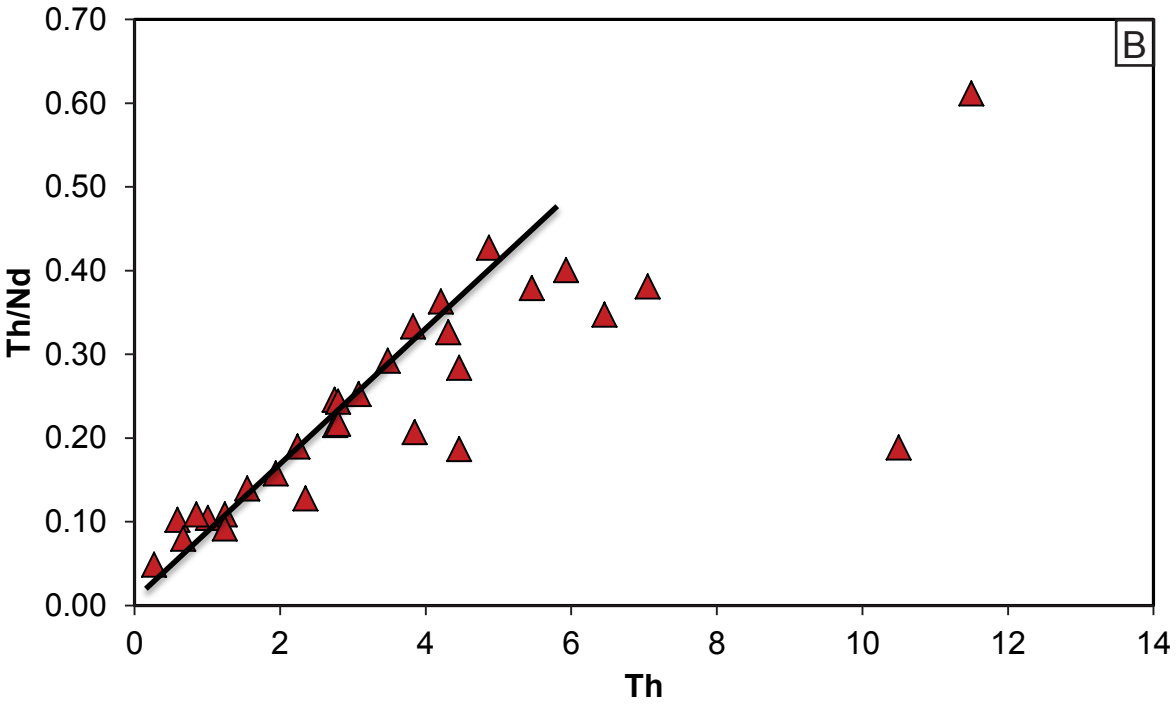

Figure 9. Bellot et al.

Figure

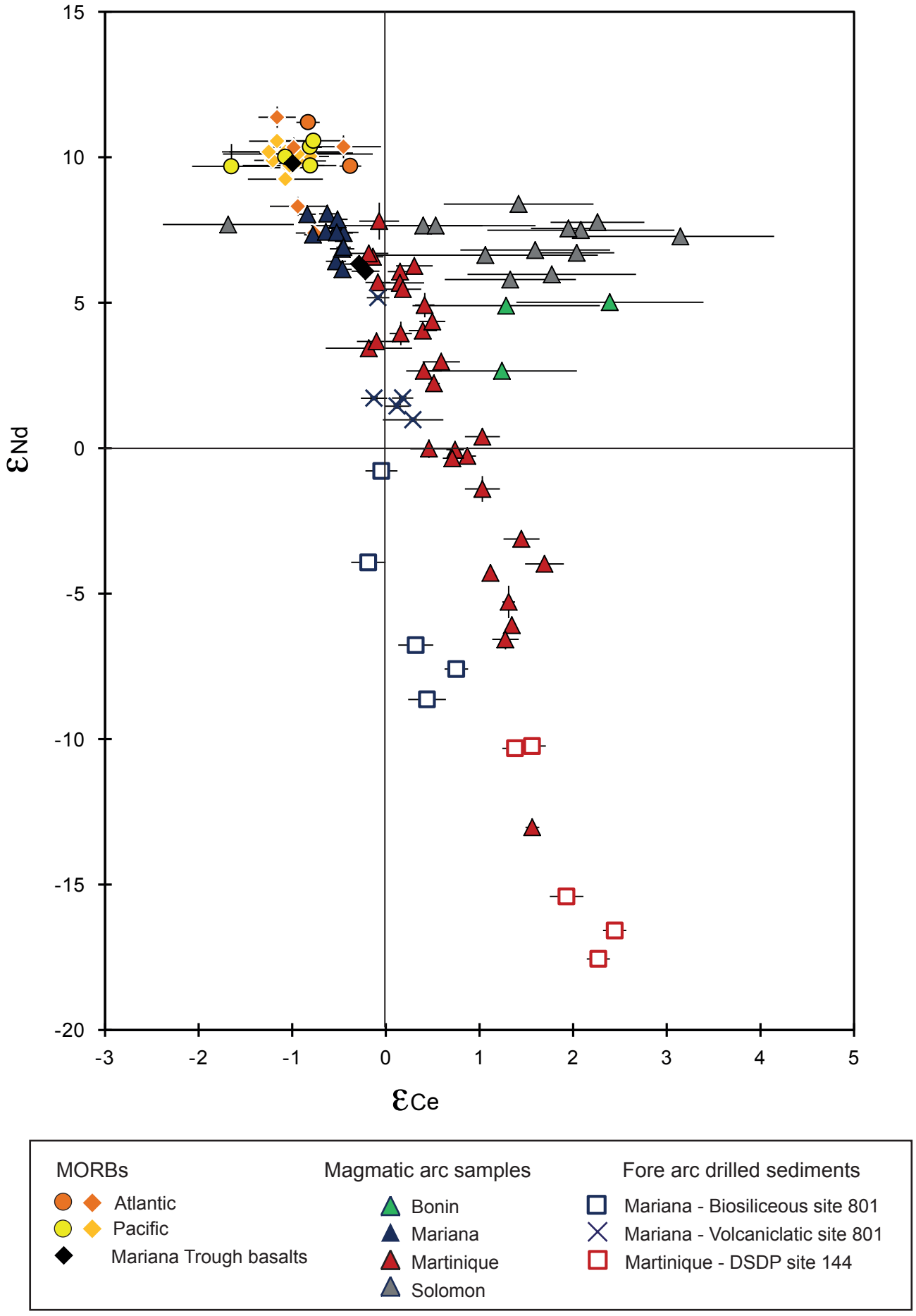

Figure 10. Bellot et al.

Figure

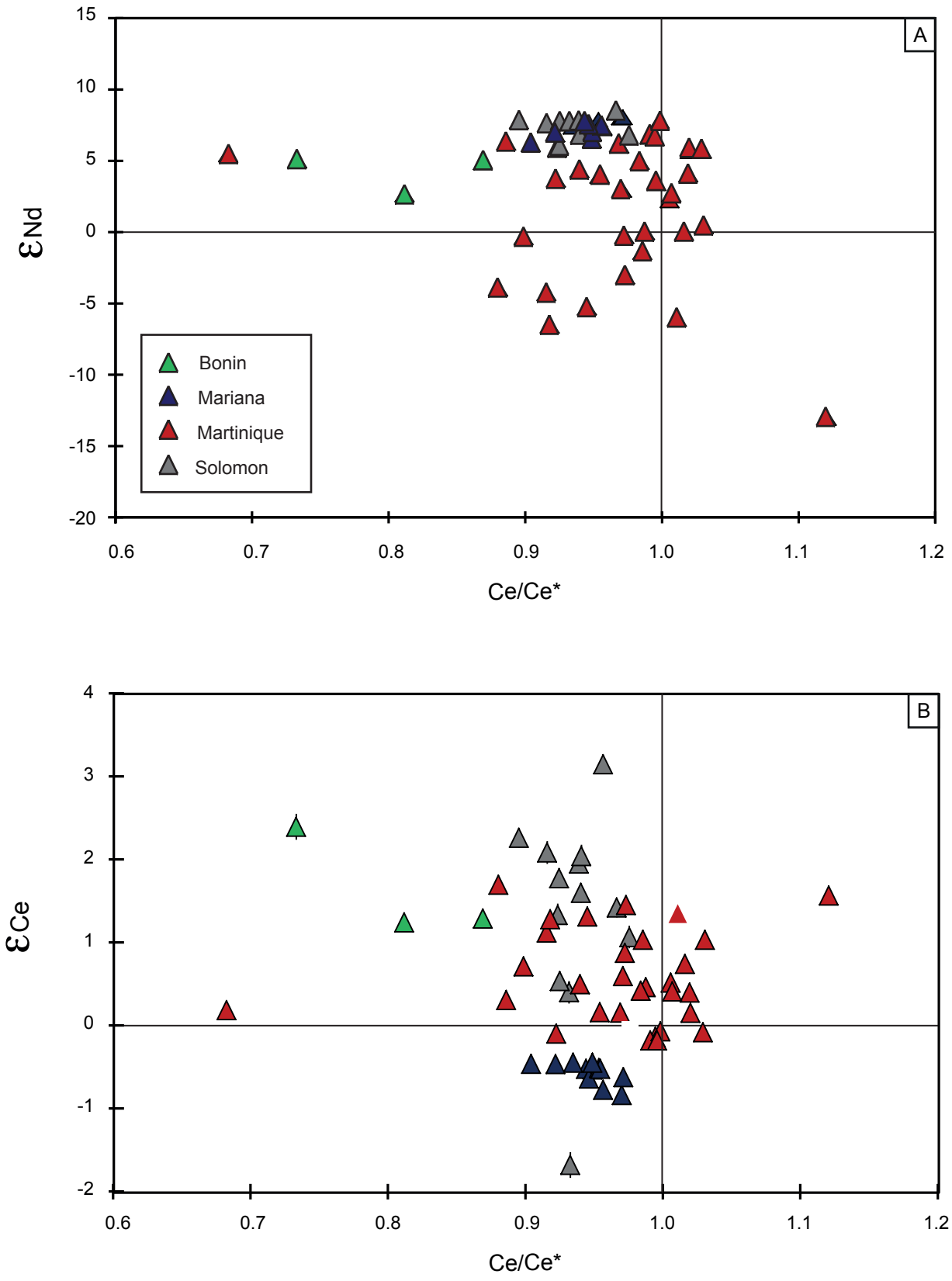

Figure 11. Bellot et al.

Table

Click here to download Table: table 1.xlsx

				Rare Earth Element concentrations in ppm													
Lavas			**SiO_2 (wt %)**	**La**	**Ce**	**Pr**	**Nd**	**Sm**	**Eu**	**Gd**	**Tb**	**Dy**	**Ho**	**Er**	**Tm**	**Yb**	**Lu**
Islands	**samples name**																
Uracas	URA5		*53.6*	5.60	12.4	1.77	8.60	2.64	0.97	3.26	0.57	3.77	0.83	2.47	0.36	2.47	0.38
	URA7		*54.2*	9.18	19.0	2.55	11.8	3.33	1.18	3.91	0.67	4.29	0.94	2.77	0.41	2.72	0.43
Asuncion	ASC3		*54.5*	5.46	12.9	1.97	9.95	3.19	1.15	3.89	0.69	4.40	0.95	2.82	0.43	2.87	0.44
Agrigan	AGR4a		*50.5*	7.78	16.3	2.35	10.9	3.01	1.06	3.21	0.54	3.26	0.67	1.97	0.29	1.92	0.29
Pagan	PAG3		*51.6*	5.36	12.5	1.89	9.40	2.87	1.04	3.44	0.59	3.72	0.79	2.35	0.34	2.30	0.35
	MM-92-10		*54.5*	11.2	24.9	3.68	17.5	5.08	1.65	5.61	0.93	5.91	1.25	3.64	0.53	3.58	0.55
Alamagan	ALAM2		*55*	6.27	14.4	2.12	10.3	3.20	0.99	3.72	0.65	4.16	0.90	2.67	0.41	2.71	0.42
	ALAM5		*53.4*	6.23	14.1	2.08	10.1	3.09	1.01	3.60	0.63	4.03	0.86	2.55	0.38	2.55	0.39
Guguan	GUG3		*51.6*	8.90	18.2	2.67	12.6	3.62	1.29	4.11	0.70	4.38	0.92	2.69	0.40	2.64	0.41
	GUG6		*51.1*	3.26	8.3	1.31	6.84	2.30	0.88	2.88	0.51	3.33	0.72	2.13	0.32	2.17	0.33
	GUG9		*51.0*	3.46	8.8	1.40	7.26	2.46	0.94	3.10	0.55	3.58	0.78	2.30	0.35	2.32	0.37
Sarigan	SAG1		*53.4*	7.44	16.5	2.37	11.3	3.34	1.14	3.77	0.64	4.11	0.88	2.58	0.38	2.57	0.39
Sediments	**Depth (mbsl)**	**Lithology**															
ODP Leg 129 Site 801A																	
8R-1-1-3-II	69	Chert	*97.9*	*21.8*	*26.2*	*5.37*	*18.2*	*3.80*	*0.91*	*4.09*	*0.62*	*3.57*	*0.72*	*1.95*		*1.73*	*0.26*
17R-1-28-30-III	155	Porcellanite	*80.4*	*17.0*	*30.1*	*4.08*	*14.1*	*2.83*	*0.74*	*2.73*	*0.42*	*2.20*	*0.41*	*1.11*		*1.00*	*0.15*
ODP Leg 129 Site 801B																	
12R-1-64-70-II	292	Porcellanite	*77.4*	10.7	22.4	2.88	12.4	2.85	0.87	3.58	0.56	3.68	0.78	2.26		2.08	0.32
5R-01W-40-42-III	232	Volc. Turbidite	*67.8*	*16.4*	*32.0*	*4.44*	*18.4*	*3.82*	*1.10*	*3.60*	*0.59*	*2.86*	*0.50*	*1.29*		*1.04*	*0.14*
7R-01W-35-37-III	251	Volc. Turbidite	*50.9*	*20.0*	*38.5*	*5.15*	*20.9*	*4.11*	*1.18*	*3.64*	*0.61*	*3.06*	*0.56*	*1.47*		*1.29*	*0.19*
8R3-115-125-III	257	Volc. Turbidite	*57.2*	*19.7*	*41.4*	*5.54*	*21.6*	*4.52*	*1.42*	*4.27*	*0.66*	*3.39*	*0.62*	*1.59*		*1.32*	*0.19*
25R-1-49-53-IV	406	Radiolarite	*86.1*	*11.8*	*19.3*	*2.95*	*9.96*	*2.04*	*0.45*	*1.94*	*0.31*	*1.71*	*0.34*	*0.95*		*0.97*	*0.15*
33R-1-143-150-IV	444	Radiolarite	*74.0*	*21.0*	*32.7*	*4.96*	*18.8*	*3.76*	*1.35*	*3.29*	*0.49*	*2.65*	*0.49*	*1.34*		*1.29*	*0.20*
ODP Leg 129 Site 802A		nannofossils+															
19R-1-27-29- II	159.4	Volc. Glass	*45*	20.8	50.8	6.52	29.0	7.15	2.37	7.42	1.11	6.33	1.16	2.98	0.38	2.33	0.32
43R-03W-33-35-V	385.43	Volc. Turbidite		23.8	45.6	6.53	27.2	5.81	1.78	5.42	0.76	4.34	0.79	2.05	0.27	1.65	0.21
Mariana Trough Basalts	**Segment**																
C7-DREDGE-3	SSP			9.98	18.7	2.58	11.7	3.13	1.06	3.54	0.55	3.48	0.73	2.12	0.31	2.08	0.31
D3-2-1	SSP		*50.4*	9.11	17.5	2.60	11.8	3.12	1.07	3.49	0.54	3.50	0.73	2.11	0.31	2.08	0.31
D68-2-1	SMT-16		*50.8*	3.28	9.91	1.74	9.30	3.14	1.18	4.24	0.71	4.77	1.01	2.94	0.42	2.74	0.40
Pacific MORB	**Latitude**	**Longitude**															
Searise 1 DR05	02°28'N	102°30'W	*50.7*	4.43	13.6	2.52	13.9	4.84	1.65	6.90	1.17	8.07	1.72	5.02	0.73	4.82	0.71
Cyana CY82	12°43'N	103°92'W		*8.94*	*22.8*	*3.33*	*15.8*	*4.23*	*1.56*	*4.99*	*0.91*	*5.77*	*1.22*	*3.44*		*3.24*	*0.49*
Clipperton DR01	12°45'N	103°56'W	*46.7*	*4.20*	*11.8*	*1.98*	*10.5*	*3.37*	*1.22*	*4.37*	*0.79*	*5.24*	*1.12*	*3.27*		*3.06*	*0.45*

Table 1

Table

Click here to download Table: table 2.xlsx

	Ce Analytical session	$^{138}Ce/^{142}Ce$	2 s.e.	ε_{Ce}	2 s.e.	$^{138}Ce/^{142}Ce$ average	ε_{Ce} average	$^{143}Nd/^{144}Nd$	2 s.e.	ε_{Nd}	2 s.e.
Lavas											
URA-5	1	0.02256410	0.00000030	-0.57	0.13	0.02256422	-0.52	0.513010	0.000003	7.40	0.06
	1	0.02256579	0.00000112	0.17	0.50						
URA-7	1	0.02256440	0.00000027	-0.44	0.12	0.02256438	-0.45	0.512980	0.000003	6.82	0.05
	1	0.02256435	0.00000036	-0.47	0.16						
ASC-3	1	0.02256457	0.00000028	-0.37	0.12	0.02256424	-0.52	0.513035	0.000002	7.90	0.05
	1	0.02256357	0.00000039	-0.81	0.17						
AGR-4a	1	0.02256434	0.00000030	-0.47	0.13			0.512983	0.000003	6.89	0.06
PAG-3	1	0.02256408	0.00000025	-0.59	0.11	0.02256395	-0.64	0.513017	0.000003	7.55	0.05
	1	0.02256383	0.00000025	-0.70	0.11						
MM92-10	1	0.02256438	0.00000022	-0.45	0.10			0.513011	0.000003	7.43	0.06
ALAM-2	1	0.02256316	0.00000032	-0.99	0.14	0.02256365	-0.78	0.513021	0.000003	7.63	0.05
	1	0.02256408	0.00000030	-0.59	0.13						
ALAM-5	1	0.02256457	0.00000028	-0.37	0.12	0.02256422	-0.52	0.513001	0.000003	7.24	0.05
	1	0.02256391	0.00000026	-0.66	0.11						
GUG-3	1	0.02256359	0.00000036	-0.80	0.16	0.02256436	-0.46	0.512938	0.000003	6.01	0.05
	1	0.02256475	0.00000026	-0.29	0.11						
GUG-6	1	0.02256299	0.00000028	-1.07	0.12	0.02256351	-0.84	0.513041	0.000003	8.02	0.05
	1	0.02256411	0.00000030	-0.57	0.13						
GUG-9	1	0.02256368	0.00000028	-0.76	0.13	0.02256399	-0.62	0.513044	0.000003	8.07	0.05
	1	0.02256430	0.00000028	-0.49	0.12						
SAG-1	1	0.02256420	0.00000024	-0.53	0.11			0.512966	0.000003	6.55	0.05
Sediments											
801A-8R (BS)	2	0.02256743	0.00000042	0.90	0.19			0.512283	0.000003	-6.77	0.06
801A-17R (BS)	2	0.02256665	0.00000042	0.55	0.18	0.02256608	0.30	0.512429	0.000003	-3.93	0.07
	2	0.02256551	0.00000041	0.05	0.18						
801B-12R (BS)	2	0.02256645	0.00000039	0.47	0.17			0.512590	0.000004	-0.79	0.07
801B-5R (Volc)	4	0.02256580	0.00000026	0.18	0.11			0.512718	0.000003	1.72	0.05
801B-7R (Volc)	4	0.02256511	0.00000032	-0.13	0.14			0.512718	0.000003	1.71	0.05
801B-8R3 (Volc)	4	0.02256605	0.00000073	0.29	0.32			0.512680	0.000003	0.97	0.06
801B-25R (BS)	2	0.02256792	0.00000035	1.12	0.15			0.512187	0.000003	-8.64	0.07
801B-33R (BS)	2	0.02256809	0.00000028	1.19	0.12	0.02256800	1.15	0.512241	0.000003	-7.60	0.06
	2	0.02256716	0.00000042	0.78	0.19						
	2	0.02256831	0.00000029	1.29	0.13						
802A-19R (Volc)	4	0.02256521	0.00000027	-0.08	0.12			0.512895	0.000003	5.17	0.06
802A-43R (Volc)	4	0.02256567	0.00000030	0.12	0.13			0.512704	0.000003	1.44	0.06
Back-arc basalts (MTB)											
C7-Dredge-3	3	0.02256513	0.00000029	-0.12	0.13	0.02256491	-0.22	0.512942	0.000002	6.08	0.05
	3	0.02256461	0.00000034	-0.35	0.15						
D3-2-1	3	0.02256532	0.00000035	-0.03	0.15	0.02256476	-0.28	0.512954	0.000002	6.33	0.04
	3	0.02256421	0.00000034	-0.53	0.15						
D68-2-1	2	0.02256375	0.00000036	-0.73	0.16	0.02256315	-1.00	0.513132	0.000003	9.79	0.06
	3	0.02256195	0.00000052	-1.53	0.23						
Pacific MORB											
Searise 1 DR05	3	0.02256365	0.00000068	-0.77	0.30			0.513171	0.000003	10.56	0.05
Cyana CY82	3	0.02256168	0.00000095	-1.65	0.42			0.513127	0.000002	9.69	0.05
Clipperton DR01	3	0.02256358	0.00000034	-0.81	0.15			0.513128	0.000003	9.71	0.05

Table 2

Table

Click here to download Table: table 3.xlsx

	La	Ce	Pr	Nd		experimental conditions	
Enrichment factor [a]	0.4	0.3	0.3	0.2	***Johnson & Plank (1999)***	**2GPa-800°C**	
Enrichment factor [a]	1.4	1.4	1.3	1.1	***Martindale et al. (2013)***	**3GPa-850°C**	
	[La] *ppm*	**[Ce] *ppm***	**[Pr] *ppm***	**[Nd] *ppm***	**Ce/Ce***	**Eps Ce**	**Eps Nd**
Depleted end-member	0.265	0.773	0.131	0.713	1.00	-1.00	9.79
BS sediment (801B-33R) derived end-member	16.4	26.1	4.00	14.7	0.78	1.15	-7.60
BS sediment (801A-17R) derived end-member	16.4	26.1	4.00	14.7	0.88	0.30	-3.93
VC sediment (801B-7R) derived end-member	20.0	39.4	5.40	22.0	0.93	-0.13	1.71
VC sediment (801B-8R3) derived end-member	20.0	39.4	5.40	22.0	0.97	0.29	0.97

Table 3

Background dataset for online publication only

Click here to download Background dataset for online publication only: Supp file A.pdf

Background dataset for online publication only

Click here to download Background dataset for online publication only: Supp file B.pdf

Background dataset for online publication only

Click here to download Background dataset for online publication only: Supp file C.pdf

Background dataset for online publication only

Click here to download Background dataset for online publication only: Supp file D.pdf

Background dataset for online publication only

Click here to download Background dataset for online publication only: Supp file E.pdf

Background dataset for online publication only

Click here to download Background dataset for online publication only: Supp file F.pdf

Background dataset for online publication only

Click here to download Background dataset for online publication only: Supp file G.pdf